Efficient random walk particle tracking algorithm for advective-dispersive transport in media with discontinuous dispersion coefficients and water contents

M. Bechtold,[1,2] J. Vanderborght,[1] O. Ippisch,[3] and H. Vereecken[1]

Received 22 November 2010; revised 5 August 2011; accepted 6 September 2011; published 26 October 2011.

[1] Random walk particle tracking (RWPT) is a well established and efficient alternative to grid-based Eulerian approaches when simulating the advection-dispersion transport problem in highly heterogeneous porous media. However, RWPT methods suffer from a lack of accuracy when the dispersion tensor or the water content is spatially discontinuous. We present improvements to the concept of a partially reflecting barrier used to account for these discontinuities: (1) the nonlinear time splitting with $\sqrt{\Delta t} = \sqrt{\Delta t_1} + \sqrt{\Delta t_2}$ that corrects for the systematic overestimation of the second dispersion displacement across an element interface when linear time splitting is used; (2) the one-sided reflection coefficient that correctly represents the effect of discontinuous dispersion coefficients and water content but eliminates redundant reflections of the two-sided reflection coefficient and limits the error for discrete Δt; and (3) the transformation of the dispersive displacement across the element interface for complex multidimensional transport problems. The proposed improvements are verified numerically by comparison with an analytical solution and a reference RWPT method. The results indicate an increased efficiency and accuracy of the new RWPT algorithm. Because the new algorithm efficiently simulates both advection- and dispersion-dominated transport conditions, it enhances the applicability of RWPT to scenarios in which both conditions occur, as, for example, in the highly transient unsaturated zone. The algorithm is easily implemented and it is shown that the computational benefit increases with increasing variability of the hydraulic parameter field.

Citation: Bechtold, M., J. Vanderborght, O. Ippisch, and H. Vereecken (2011), Efficient random walk particle tracking algorithm for advective-dispersive transport in media with discontinuous dispersion coefficients and water contents, *Water Resour. Res., 47*, W10526, doi:10.1029/2010WR010267.

1. Introduction

[2] The increasing knowledge about subsurface heterogeneity and its crucial effects on water flow and solute transport led to highly resolved numerical models at different scales [*Coquet et al.*, 2005; *Javaux et al.*, 2006; *Kasteel et al.*, 2007]. This development increased the computational costs of numerical simulations. At the same time, inverse modeling studies of multidimensional flow and transport problems, like geostatistical inversions, become more frequent [e.g., *Kowalsky et al.*, 2004; *Nowak et al.*, 2010]. These studies require multiple forward runs of computationally expensive simulations. Both developments result in an ongoing demand for efficient modeling codes, despite the availability of more powerful computers.

[3] There is a long discussion about the most efficient and robust concepts for modeling solute transport in highly heterogeneous porous media [*Delay et al.*, 2005]. Two different concepts are mostly used to numerically solve the advection-dispersion equation (ADE): (1) grid-based Eulerian and (2) Lagrangian approaches. Among the Lagrangian approaches, the most common one is the random walk particle tracking (RWPT). This method is based on the analogy between stochastic processes and diffusion theory [*Kinzelbach and Uffink*, 1991]. Applied to solute transport problems, the solute mass is represented by a large number of particles. Fundamental works in stochastic physics demonstrated the similarity between ADE and the Fokker-Planck equation, which describes the temporal evolution of the probability density function of the particle velocity [*Delay et al.*, 2005]. Based on this similarity, in RWPT, particles perform displacements that are composed of an advective (deterministic) and a dispersive (stochastic) component, whereby the advective movement is the sum of the fluid flow velocity and the velocity that originates from the spatial continuous variation of the dispersion tensor and water content [*LaBolle et al.*, 1996]. In the limit of an infinite number of particles, the resulting frequency distribution equals a solution of the Fokker-Planck equation, and thus also a solution of the ADE.

[4] In subsurface hydrology, RWPT methods were first applied to groundwater flow problems [*Ahlstrom et al.*, 1977; *Prickett et al.*, 1981]. For advection-dominated transport problems, in which grid-based Eulerian methods

[1]Agrosphere (IBG-3), Institute of Bio- and Geosciences, Forschungszentrum Jülich GmbH, Jülich, Germany.
[2]Institute of Agricultural Climate Research, Johann Heinrich von Thünen-Institut (vTI), Braunschweig, Germany.
[3]Interdisciplinary Center of Scientific Computing, University of Heidelberg, Heidelberg, Germany.

0043-1397/11/2010WR010267

suffer from numerical diffusion, they became a well established alternative for modeling subsurface transport [e.g., *Fernandez-Garcia et al.*, 2005; *LaBolle et al.*, 1996; *Maxwell et al.*, 2007; *Park et al.*, 2008; *Tompson and Gelhar*, 1990]. For these conditions, RWPT is considered to be more efficient in providing accurate results because the grid-based Eulerian approaches require a computational expensive grid refinement and time step reduction to overcome numerical diffusion [*Lichtner et al.*, 2002; *Salamon et al.*, 2006].

[5] Recently, *Delay et al.* [2005] pointed out that RWPT has rarely been used in vadose zone hydrology, although high variations in water content and flow velocity are very common for the vadose zone, and RWPT is supposed to efficiently model transport under these conditions. RWPT can also be an attractive alternative for handling high concentration gradients due to solute accumulation either at the soil surface caused by evaporation or at the roots caused by root water uptake, scenarios which are posing very high demands on the numerical solution scheme. Recently, it has been shown that RWPT can be used to efficiently simulate large-scale contaminant transport problems in coupled unsaturated/saturated domains [*Maxwell et al.*, 2009].

[6] RWPT methods are by definition globally mass conservative, which is an important advantage of the method compared to most finite-element and finite-difference schemes. However, a difficulty of the RWPT method is that locally, the particle displacements are erroneous when the dispersion tensor or the water content is spatially discontinuous. Such discontinuities result from abrupt changes of the physical properties of the porous material (e.g., at abrupt facies changes or local compaction zones) or from characteristics of the computed velocity field obtained from a numerical model such as cell-centered finite volume-based flow models [*Delay et al.*, 2005; *Salamon et al.*, 2006]. When neglecting these discontinuities, RWPT simulations may provide transport results with considerable errors [*LaBolle et al.*, 1996].

[7] Methods that reduce the errors related to the discontinuities are frequently debated in RWPT literature and are the topic of this study. There were three conceptually different methods proposed: the interpolation method [*LaBolle et al.*, 1996], the generalized stochastic differential equations (GSDE) method [*LaBolle et al.*, 2000], and the concept of a partially reflecting barrier [*Hoteit et al.*, 2002; *Lim*, 2006]. In these methods, algorithmic modifications were introduced to the performance of the advective and dispersive displacements. The modified algorithms lead to different particle frequency distributions in the presence of discontinuities and to a better approximation of the true solution of the ADE.

[8] While the interpolation method and the GSDE method were successfully applied to complex three-dimensional transport problems [e.g., *Fernandez-Garcia et al.*, 2005; *Salamon et al.*, 2007; *Seeboonruang and Ginn*, 2006; *Weissmann et al.*, 2002], the general applicability of the reflection barrier method and its convergence to the true solution is controversially discussed [*Salamon et al.*, 2006]. Based on a comparison study, *Salamon et al.* [2006] proposed that the interpolation method presented the most efficient alternative for most of the complex three-dimensional flow problems, especially with respect to scenarios characterized by low fluid velocities and abrupt contrasts.

[9] However, it is well known that the interpolation method needs a very high spatial resolution of the interpolation grid close to the interface and small time steps [*LaBolle et al.*, 1996], which is computationally expensive. The reflection barrier method does not require grid refinement to represent discontinuous dispersion tensors or abrupt changes in the water content. This advantage can reduce computational costs considerably. It is therefore promising to improve the accuracy of the reflection barrier method and to prove its general applicability.

[10] This manuscript is organized as follows. In section 2, we will briefly review the interpolation and reflection barrier method as they are currently implemented in transport codes. For the reflection barrier method, we identify some problems and inconsistencies with respect to its implementation, which may explain why the reflection barrier method was outperformed by other methods in the comparison study of *Salamon et al.* [2006]. Based on the identified inconsistencies, we will propose improvements to the reflection barrier method. In section 3, we discuss details about the numerical implementation of the reflection barrier method and describe and motivate the test scenarios used for the numerical verification of the proposed RWPT algorithm. In section 4, we use the numerical results to evaluate the benefit of the improved algorithm. The improved reflection barrier method is compared with the interpolation method [*LaBolle et al.*, 1996]. In section 5, convergence and efficiency issues are discussed and we will provide practical application aspects of the new algorithm. Conclusions are provided in section 6.

2. Theory

2.1. Reflection Barrier and Interpolation Method

[11] In porous media, the mass balance equation of a conservative solute is described by the advection-dispersion equation (ADE),

$$\theta \frac{\partial C}{\partial t} = -\theta \mathbf{u} \times \nabla C + \nabla \times (\theta \mathbf{D} \times \nabla C), \tag{1}$$

where θ is the volumetric water content ($L^3\ L^{-3}$), C is the concentration ($M\ L^{-3}$), t is time (T), $\mathbf{u}$ is the velocity vector ($L\ T^{-1}$), and $\mathbf{D}$ is the local-scale dispersion tensor ($L^2\ T^{-1}$), here given for a three-dimensional isotropic porous medium [*Bear*, 1972],

$$\mathbf{D} = (\alpha_T \|\mathbf{u}\| + D_m)\mathbf{I} + (\alpha_L - \alpha_T)\frac{\mathbf{u}\mathbf{u}^T}{\|\mathbf{u}\|}, \tag{2}$$

where α_T and α_L are the transversal and longitudinal dispersivities (L), D_m is the effective molecular diffusion coefficient ($L^2\ T^{-1}$), and $\mathbf{I}$ is the identity matrix. The stochastic differential equation equivalent to the ADE can be written as [*Tompson and Gelhar*, 1990],

$$\mathbf{X}(t+\Delta t) = \mathbf{X}(t) + \left[\mathbf{u}[\mathbf{X}(t)] + \nabla \times \mathbf{D}[\mathbf{X}(t)] + \frac{\mathbf{D}[\mathbf{X}(t)]}{\theta[\mathbf{X}(t)]} \times \nabla\theta[\mathbf{X}(t)]\right]\Delta t + \mathbf{B}[\mathbf{X}(t)]\boldsymbol{\xi}\sqrt{\Delta t}, \tag{3}$$

where $\mathbf{X}$ is the coordinate vector (L), $\boldsymbol{\xi}$ is a vector of three random numbers normally distributed with zero mean and unit variance, and $\mathbf{B}$ is the dispersion displacement matrix [*Lichtner et al.*, 2002],

$$\mathbf{B} = \begin{pmatrix} \frac{u_x}{\|\mathbf{u}\|}\sqrt{2(\alpha_L\|\mathbf{u}\| + D_m)} & -\frac{u_x u_z}{\|\mathbf{u}\|\sqrt{u_x^2+u_y^2}}\sqrt{2(\alpha_T\|\mathbf{u}\| + D_m)} & -\frac{u_y}{\sqrt{u_x^2+u_y^2}}\sqrt{2(\alpha_T\|\mathbf{u}\| + D_m)} \\ \frac{u_y}{\|\mathbf{u}\|}\sqrt{2(\alpha_L\|\mathbf{u}\| + D_m)} & -\frac{u_y u_z}{\|\mathbf{u}\|\sqrt{u_x^2+u_y^2}}\sqrt{2(\alpha_T\|\mathbf{u}\| + D_m)} & \frac{u_x}{\sqrt{u_x^2+u_y^2}}\sqrt{2(\alpha_T\|\mathbf{u}\| + D_m)} \\ \frac{u_z}{\|\mathbf{u}\|}\sqrt{2(\alpha_L\|\mathbf{u}\| + D_m)} & \frac{\sqrt{u_x^2+u_y^2}}{\|\mathbf{u}\|}\sqrt{2(\alpha_T\|\mathbf{u}\| + D_m)} & 0 \end{pmatrix}, \quad (4)$$

where u_x, u_y, and u_z are the velocities in x-, y-, and z-direction, and $\|\mathbf{u}\|$ is the Euclidean norm of the velocity. For diffusion-only problems or when $u_x = u_y = 0$, $\mathbf{B}$ is obtained by taking the limit of $\mathbf{B}$ for the respective velocity components going to zero, which is well defined. Using the central limit theorem, the normal random vector ξ of equation (3) can be replaced by $\sqrt{3}\mathbf{Z}$ where $\mathbf{Z}$ is a random vector uniformly distributed between -1 and 1, which has been shown to be computationally more efficient [*Uffink*, 1985]. The term $\left[\mathbf{u}[\mathbf{X}(t)] + \nabla \times \mathbf{D}[\mathbf{X}(t)] + \frac{\mathbf{D}[\mathbf{X}(t)]}{\theta[\mathbf{X}(t)]} \times \nabla\theta[\mathbf{X}(t)]\right]$ of equation (3) is responsible for the advective (deterministic) movement of a particle, which is the sum of the fluid velocity and a velocity that originates from the spatial variation of $\mathbf{D}$ and θ [*LaBolle et al.*, 1996]. The term $\mathbf{B}[\mathbf{X}(t)]\xi\sqrt{\Delta t}$ represents the dispersive (stochastic) movement.

[12] When equation (3) is applied to a large number of particles, the resulting particle distributions mimic the Fokker-Planck equation and thus provide a solution to the ADE [*Delay et al.*, 2005]. However, RWPT algorithms need an additional adaptation when the terms of equation (3) accounting for continuous spatial variations of the dispersion tensor and water content are not defined, i.e., the dispersion tensor or the water content are discontinuous [*LaBolle et al.*, 1996, 1998]. Linear parabolic partial differential equations like the ADE should obey a maximum principle when a mass-conservative flow field is used. This means that the maxima (and minima) of concentration are either at the inflow boundaries or in the initial condition. Over time no new extremes are created, as the linear transport conserves the shape of a concentration pulse and diffusion tends to diminish extreme values. This property should be retained by any reasonable numerical scheme. Of course for RWPT methods this can only be true in a statistical sense, i.e., no new extremes larger than the pure statistical fluctuations due to the discretization error should be introduced. If discontinuities of the dispersion tensor and/or the water content are neglected, this is no longer guaranteed, resulting in potentially very large solute concentrations in low dispersion regions. This effect has been previously reported as "local mass conservation error" [*LaBolle et al.*, 1996; *Semra et al.*, 1993]. However, as particle tracking methods are by definition mass conservative, we prefer to call it "monotonicity preservation error" in this paper, in reference to the potential violation of the maximum principle.

[13] Before introducing the interpolation and reflection barrier method, which were both developed to avoid "monotonicity preservation errors" because of discontinuities in $\mathbf{D}$ or θ, it is necessary to define the use of grids in RWPT. Primarily, RWPT is a grid-free method. For purely advective transport, convergence to the true solution is achieved by accurately integrating the velocity along the trajectory of each particle and by decreasing the mass of the individual particles representing the total solute mass, while increasing the total number of particles. For advective-dispersive transport, convergence also requires a sufficiently small time step. However, numerical grids are required when the spatially varying variables governing the particle displacements (in this study: velocity, dispersion tensor, and water content) cannot be described analytically at each location, but must be obtained from a grid-based numerical solution of the flow problem. Numerical grids are used in RWPT algorithms to obtain the variables at the particle location by adequate interpolation functions [*LaBolle et al.*, 1996]. Grids are also often used to derive solute concentrations from the particle distributions. However, in the following, we refer to the first type of grids when we discuss the effect of grid refinement on the numerical solution of RWPT.

[14] In the interpolation method, the discontinuity in the dispersion tensor or the water content is replaced by a smooth transition interpolating the discontinuous values. This introduces an error which gets smaller with decreasing size of the interpolation region. The interpolation method is commonly used as a "hybrid" scheme [*LaBolle et al.*, 1996]. In this scheme, the term $\mathbf{u}\Delta t$ is calculated from the flow solution in the same way as in a standard particle-tracking scheme. Bilinear interpolation is used for the calculation of the terms $\left[\nabla \times \mathbf{D}[x(t)] + \frac{\mathbf{D}[x(t)]}{\theta[x(t)]} \times \nabla\theta[x(t)]\right]\Delta t$ and $\mathbf{B}[\mathbf{X}(t)]\xi\sqrt{\Delta t}$ of equation (3). This scheme maintains the local fluid mass balance from the flow solution, while the smoothed field allows the approximation of the divergence of the dispersion tensor and of the gradient of the water content in the vicinity of the discontinuity. Any smoothing error by the bilinear interpolation of the velocities and water contents affects the terms with $\mathbf{D}$, $\mathbf{B}$, and θ. Convergence is achieved by refinement of the interpolation grid to reduce the smoothing zone at the discontinuity. This also requires a simultaneous time step reduction to allow particles to explore the smoothing zone.

[15] Another approach to account for discontinuous dispersion tensors and water contents is the concept of a partially reflecting barrier, first introduced by *Uffink* [1985]. The advective displacement is calculated from the flow solution and performed in the same way as in a standard RWPT scheme that accounts for continuous changes of $\mathbf{D}$ and θ. Subsequently, the dispersive displacement accounts for the discontinuous changes of $\mathbf{D}$ and θ. The fundamental principle of the reflection barrier concept is to partially reflect particles that cross the discontinuity during the dispersive displacement. The difficulty is to design this reflection barrier in such a way that the correct solution of the

ADE is obtained. This concept is basically implemented by generating an additional random number when a particle reaches an element interface during a specific displacement. If the random number is greater than the reflection coefficient, the particle crosses the interface; otherwise, it is reflected. An important advantage of the reflection barrier method is that it does not require a finer spatial discretization close to the interface and thus can operate with larger time steps.

[16] After the reflection barrier method was introduced by *Uffink* [1985] several concepts were proposed [e.g., *Cordes et al.*, 1991; *LaBolle et al.*, 1998; *Semra et al.*, 1993] which differ in the definition of (1) the reflection coefficient and (2) the length of the displacement for a particle which crosses the interface [*Ackerer and Mose*, 2000]. The reflection scheme that is now generally considered as the only one that preserves monotonicity was first presented by *Semra et al.* [1993]. It was validated by *Hoteit et al.* [2002] and is now mostly known as the reflection scheme of *Hoteit et al.* [2002]. Recently, *Ramirez et al.* [2008] referred to this scheme as the Hoteit-Mose-Younes-Lehmann-Ackerer reflection (HMYLA reflection).

[17] In the scheme of *Hoteit et al.* [2002], which was developed for a medium with a homogeneous water content, the probability that a particle that reached, during a dispersive displacement, the interface between two elements E_1 and E_2 with dispersion coefficients D_1 and D_2 goes into E_1 is $P_1 = \frac{\sqrt{D_1}}{\sqrt{D_1}+\sqrt{D_2}}$ and the probability that a particle goes into E_2 is $P_2 = 1 - P_1 = \frac{\sqrt{D_2}}{\sqrt{D_1}+\sqrt{D_2}}$. P_1 can also be interpreted as the probability that a particle that reaches the interface during a dispersive displacement from E_2 will enter E_1 and vice versa for P_2. The reflection coefficient has to be applied for particles coming to the interface from both directions (see also Figure 1). Recently, *Ramirez et al.* [2008] provided a physical foundation for the reflection coefficients of *Hoteit et al.* [2002] on the basis of the α-skew Brownian motion theory. *Lim* [2006] determined from the analytical solution for diffusion in a composite porous medium an extended reflection coefficient for heterogeneous effective porosities or water contents θ, where:

$$P_1 = \frac{\theta_1\sqrt{D_1}}{\theta_1\sqrt{D_1}+\theta_2\sqrt{D_2}} \text{ and } P_2 = 1 - P_1 = \frac{\theta_2\sqrt{D_2}}{\theta_1\sqrt{D_1}+\theta_2\sqrt{D_2}}. \quad (5)$$

[18] In the case of reactive transport, where E_1 and E_2 are characterized by retardation factors R_1 and R_2 ($R > 1$), D_1 and D_2 can be replaced by D_1/R_1 and D_2/R_2, respectively [*Lim*, 2006]. When the particle crosses an interface by a dispersive displacement during a time step having the size Δt, the particle displacement needs to be split up in two steps. As proposed by *Hoteit et al.* [2002] and presented in subsequent studies [e.g., *Delay et al.*, 2005; *Lim*, 2006; *Salamon et al.*, 2006], Δt is split linearly with $\Delta t = \Delta t_1 + \Delta t_2$, where Δt_1 is the time needed for the particle to reach the interface. At the element interface, the reflection coefficient is calculated and if the random number allows the particle to pass, the displacement in the next element is calculated based on the dispersion and velocity of E_2 using Δt_2. This splitting of the displacement is considered as an important precondition for preserving monotonicity [*Ackerer and Mose*, 2000]. However, we will show that a linear time splitting, which is correct for an advective

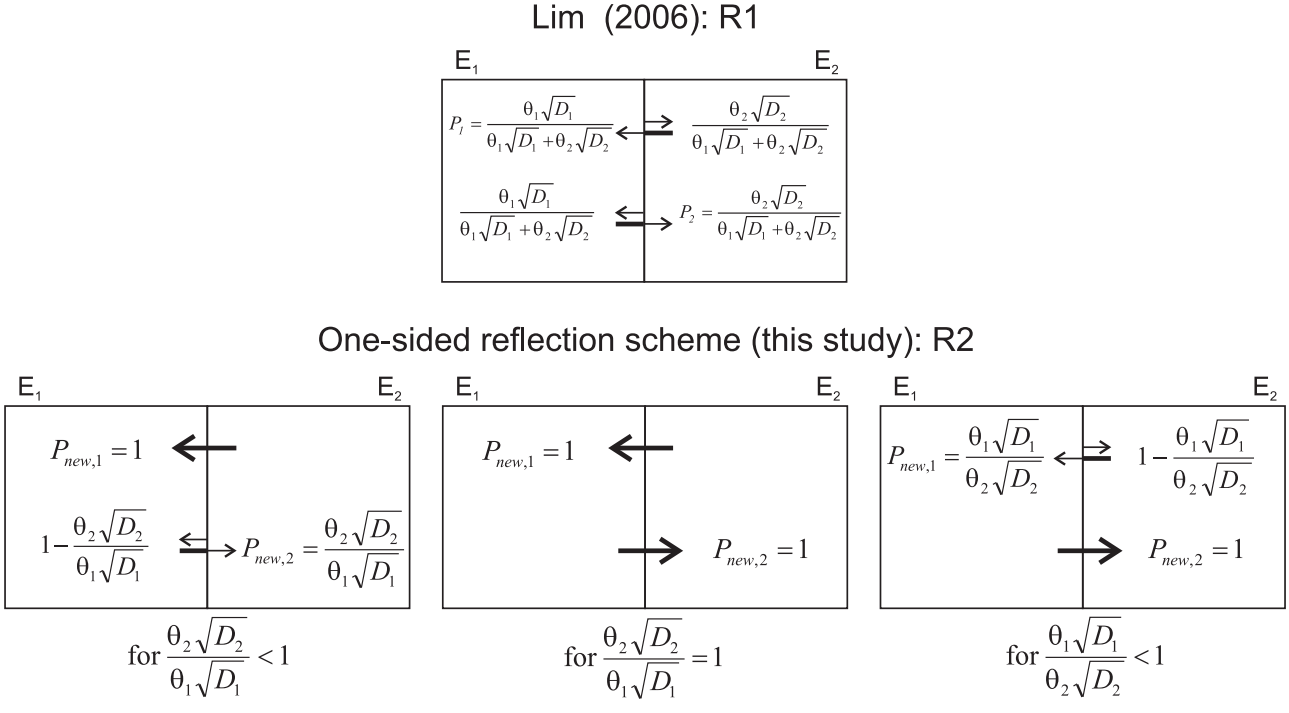

Figure 1. Summary of the reflection coefficients, R1: [*Lim*, 2006] and R2 (one-sided reflection scheme, this study), used in the numerical simulations. The fraction of the particles that is passed or reflected is indicated at the tip of each arrow. P_1 and $P_{new,1}$ are interpreted as the probability that a particle that reaches the interface from E_2 will enter E_1 and vice versa for P_2.

displacement, causes a systematic overestimation of the second dispersive displacement. In section 2.2, we derive the correct equation for determining Δt_2.

[19] A second problem of the reflection barrier method as proposed by *Hoteit et al.* [2002] and *Lim* [2006] is that even in homogeneous media, i.e., $D_1 = D_2$ and $\theta_1 = \theta_2$, particles are reflected at element interfaces. We will show that these reflections slow down the dispersive spreading of a solute pulse and that the reflection barrier method only leads to correct results when the ratio of particle displacements with reflection to the particle displacements without reflection goes to 0. This is the case when the distance between partially reflecting element interfaces $\Delta L \rightarrow \infty$ or the time step $\Delta t \rightarrow 0$. We will present an alternative reflection scheme that reduces the number of particle reflections and therefore leads to more accurate results for larger values of Δt or smaller values of ΔL.

[20] Finally, we propose a third improvement to the reflection barrier method: the transformation of the dispersive displacement when a particle crosses the interface during a dispersive displacement. We show that the transformation improves the application of the reflection barrier method in complex multidimensional transport problems with spatially varying anisotropic dispersion tensors.

2.2. Improvements to the Reflection Barrier Method

[21] All displacement and reflection probabilities considered in the following refer only to purely dispersive, i.e., stochastic, displacements. This implies that the advective and dispersive displacement must be performed in two subsequent displacement steps, i.e., the dispersive displacement is calculated at the new particle location at the end of the advective movement.

2.2.1. Correct Time Splitting for Dispersion

[22] If a particle is allowed to cross the interface of two elements with different dispersion tensor or water content, the dispersive displacement in the new element has to be recalculated consistent with the reflection coefficient to obtain a correct solution of the ADE [*Ackerer and Mose*, 2000; *Hoteit et al.*, 2002]. To be consistent with the reflection coefficient, the ratio of the mean lengths of the dispersive displacements toward and away from the interface must be equal to the ratio of the square root of the dispersion coefficients according to the reflection barrier theory of *Hoteit et al.* [2002]. If this is not the case, particles end up at an erroneous distance to the interface and the probability of a back jump in the next step would be too high or too low, with the consequence that the dispersive displacements across the element interface are not balanced accurately. In case of a particle reflection, there is no need for recalculating the dispersive displacement. The remaining displacement is performed in the opposite direction.

[23] There are two reasons that indicate that the same random number must be used for the second displacement. Both reasons are related to the fact that the subset of random numbers that cause a displacement to the interface describes a frequency distribution that differs from the original one. First, the numbers of this subset are either all positive or all negative. If a new random number would be drawn at the element interface, 50% of the random numbers would cause an immediate back jump, which is inconsistent with the reflection barrier. In contrast, using the same number ensures a displacement in the same direction like the first displacement and thus away from the interface into the new element. Second, there is higher probability that particles with higher random numbers are displaced to the interface. At the interface, however, only part of the individual random number already took effect. By drawing a new random number, the remaining fraction would be ignored. This would lead to an average of $\xi\sqrt{\Delta t}$ that is unequal to 0, because the Δt of high random numbers would be inevitably smaller in the respective direction. This would introduce an undesired bias, because, in this case, ξ would contain a part that could be added to the deterministic movement.

[24] However, keeping the random number has important consequences for the splitting of the time step at the interface. The total dispersive displacement ΔX across an element interface can be split in two displacements: ΔX_1 and ΔX_2, where ΔX_1 is the displacement to and ΔX_2 is the displacement from the element interface with:

$$\Delta X_1 = \xi\sqrt{2D_1\Delta t_1} \text{ and } \Delta X_2 = \xi\sqrt{2D_2\Delta t_2}. \tag{6}$$

[25] For the homogeneous case with $D = D_1 = D_2$, a reflection barrier is in fact not necessary, but can be used to evaluate the effect of a time splitting. Obviously, ΔX is overestimated when we recalculate the dispersion step at the interface by splitting up the time step linearly with $\Delta t = \Delta t_1 + \Delta t_2$, as it is done up to now in the reflection barrier method, as

$$\Delta X = \xi\sqrt{2D(\Delta t_1 + \Delta t_2)} < \xi\sqrt{2D\Delta t_1} + \xi\sqrt{2D\Delta t_2}. \tag{7}$$

[26] To be consistent with the definition of the reflection coefficient in the homogenous case, the total dispersive displacement calculated at the starting location, however, must be equal to the sum of the split dispersive displacements:

$$\xi\sqrt{2D\Delta t} = \xi\sqrt{2D\Delta t_1} + \xi\sqrt{2D\Delta t_2}. \tag{8}$$

[27] This simplifies to the nonlinear time-splitting equation,

$$\sqrt{\Delta t} = \sqrt{\Delta t_1} + \sqrt{\Delta t_2}. \tag{9}$$

[28] As Δt_1 is an unknown but ΔX_1 a known variable, we insert $\sqrt{\Delta t_1} = \frac{\Delta X_1}{\xi\sqrt{2D_1}}$ in equation (9) and solve for Δt_2,

$$\Delta t_2 = \left(1 - \frac{\Delta X_1}{\xi\sqrt{2D_1\Delta t}}\right)^2 \Delta t. \tag{10}$$

[29] This new time splitting scheme is straightforward to implement in a particle-tracking code. Equation (9) is equally applicable for the heterogeneous case.

2.2.2. One-sided Reflection Coefficient

[30] Let us assume that the pore water concentrations of two elements E_1 and E_2 are equal, but the volumetric water contents are different (e.g., 10 particles in E_1 with a water content of 0.25, and 20 particles in E_2 with a water content of 0.5). To preserve monotonicity, the number of particles that cross the element interface from E_1 into E_2 by dispersive displacements should, on average, be equal to the number of particles that cross from E_2 into E_1, independent of the dispersion coefficients and water contents in the two elements.

If the dispersion coefficients and volumetric water contents in E_1 and E_2 are different, the probability β_1 that a particle from E_1 reaches the interface is different from the probability β_2 that a particle from E_2 reaches the interface, which is the case also for identical pore water concentrations in E_1 and E_2. The reflection coefficients P_1 and P_2 (see above) correct for the difference in probability β_1 and β_2 so that for the same pore water concentrations in E_1 and E_2, the same amount of particles cross from E_2 into E_1 as from E_1 to E_2,

$$P_2\beta_1 = \frac{\theta_2\sqrt{D_2}}{\theta_1\sqrt{D_1}+\theta_2\sqrt{D_2}}\beta_1 = \frac{\theta_1\sqrt{D_1}}{\theta_1\sqrt{D_1}+\theta_2\sqrt{D_2}}\beta_2 = P_1\beta_2. \tag{11}$$

[31] In this two-sided reflection scheme, particles coming from both E_1 and E_2 are reflected at the interface with different reflection probabilities P_1 and P_2. Note that even in a homogeneous medium ($D_1 = D_2$ and $\theta_1 = \theta_2$) 50% of the particles are reflected at any interface between two elements, though no reflections would be needed at all to preserve monotonicity.

[32] Instead of always reflecting a fraction of the particles at both sides of the interface, it is possible to obtain the same result by reflecting an adjusted portion of particles at one side only. The reflection coefficients can be redefined by rewriting equation (11) as

$$\beta_2 = \frac{\theta_2\sqrt{D_2}}{\theta_1\sqrt{D_1}}\beta_1 \text{ or } \beta_1 = \frac{\theta_1\sqrt{D_1}}{\theta_2\sqrt{D_2}}\beta_2. \tag{12}$$

[33] The reflection coefficients are then given as

$$P_{\text{new},1} = 1 \text{ and } P_{\text{new},2} = \frac{\theta_2\sqrt{D_2}}{\theta_1\sqrt{D_1}} \quad \text{for} \quad \frac{\theta_2\sqrt{D_2}}{\theta_1\sqrt{D_1}} < 1 \tag{13}$$

or

$$P_{\text{new},2} = 1 \text{ and } P_{\text{new},1} = \frac{\theta_1\sqrt{D_1}}{\theta_2\sqrt{D_2}} \quad \text{for} \quad \frac{\theta_1\sqrt{D_1}}{\theta_2\sqrt{D_2}} \le 1, \tag{14}$$

where $P_{\text{new},1}$ is the probability that a particle that reaches the interface coming from E_2 crosses into E_1, and $P_{\text{new},2}$ the probability that a particle that reaches the interface coming from E_1 crosses into E_2 (see also Figure 1).

[34] The elimination of the reflection coefficient at one of the sides is balanced by a reduction of the reflected particles at the other side. Thus, the number of particles affected by the reflection is always smaller when applying the one-sided reflection scheme compared to the two-sided reflection coefficients of *Hoteit et al.* [2002] and *Lim* [2006]. The elimination of redundant reflections is beneficial as each reflection causes a numerical error. The reason for the error can be easily understood considering the case of a medium with a homogeneous dispersion but with an interface between two elements. When initially all particles are at one side of the interface, the two-sided reflection scheme will reduce the portion of particles that moves into the other side of the interface (because 50% are reflected) and will therefore reduce the effective dispersion, resulting in a slow convergence with a decreasing time step size. The one-sided reflection scheme does not introduce reflections at the interface between two elements in a homogeneous medium and therefore does not lead to errors in the prediction of the spreading of particles in such a medium. Therefore, it is more efficient to use the one-sided reflection scheme. We will show that the one-sided reflection scheme can reduce modeling errors tremendously, especially for large time steps.

2.2.3. Transformation of the Dispersive Displacement

[35] If the dispersion coefficient is not a scalar but a tensor, a more elaborate transformation of the dispersive displacement in the second element, $\Delta\mathbf{X}_2$, than $\Delta\mathbf{X}_2 = \boldsymbol{\xi}\mathbf{B}_2\sqrt{\Delta t_2}$, which would be expected for a scalar dispersion coefficient according to equation (6), is necessary. This can be illustrated by a simple two-layer example. This scenario can be considered as a soil above an aquifer. In the upper layer (soil), the velocity, u_z, is directed vertically downward equal to -1 m d^{-1} and in the lower layer (aquifer), the velocity, u_x, is parallel to the x-axis with a value equal to 1 m d^{-1}. Both layers have a longitudinal dispersivity $\alpha_L = 10$ m and a transverse dispersivity $\alpha_T = 1$ m. The corresponding dispersive displacement matrices $\mathbf{B}_1$ (soil) and $\mathbf{B}_2$ (aquifer) are given for the three-dimensional case according to equation (4), as

$$\mathbf{B}_1 = \begin{pmatrix} 0 & 1 & -1 \\ 0 & 1 & 1 \\ -\sqrt{20} & 0 & 0 \end{pmatrix} \quad \text{and} \quad \mathbf{B}_2 = \begin{pmatrix} \sqrt{20} & 0 & \\ 0 & 0 & \sqrt{2} \\ 0 & \sqrt{2} & 0 \end{pmatrix}.$$

[36] In this example, we only consider the interface between the two layers, thus, dimensions and boundary conditions are not relevant. Dispersive displacements in the direction perpendicular to the interface of particles in the upper layer depend only on the first entry of the random vector $\boldsymbol{\xi}$, ξ_1 (equation (3)). Because the probability that a particle reaches the interface by a dispersive displacement during a single time step Δt is increased with positive, high random numbers, the subset of random vectors $\boldsymbol{\xi}_{\text{sub}}$ leading to a displacement to the interface will be characterized by $\bar{\xi}_{\text{sub},1} > \bar{\xi}_{\text{sub},2} = \bar{\xi}_{\text{sub},3} = 0$, where the overbar refers to the mean value of the subset of random numbers. Dispersive displacements perpendicular to the interface of particles in the lower layer depend only on the second entry of $\boldsymbol{\xi}$, ξ_2. Since the dispersive displacement in the z-direction in the upper layer does not depend on ξ_2, $\bar{\xi}_{\text{sub},2}$ is 0. Using the same set of random numbers for the second part of the displacement in the lower layer halve of the particles that are allowed to pass, i.e., the ones with $\xi_{\text{sub},2} > 0$, will be displaced back into the upper layer resulting in a bias of the particle distribution. Additionally, $\bar{\xi}_{\text{sub},1} > 0$ will lead to a positive mean of dispersive displacements in the horizontal direction in the lower layer, which is implausible because the mean of these dispersive displacements is supposed to be 0.

[37] This simple example illustrates that the set of random numbers that led to a displacement to the interface in the first layer needs to be modified in order to calculate the dispersive displacement in the second layer in a correct manner. A better solution is obtained if the total displacements resulting from the random numbers in the first element are used as a basis to calculate the displacements in the second element. We first treat the displacements in the direction perpendicular, i = j, to the interface and afterward

the displacements parallel to the interface, i ≠ j (with i = x,y,z and j = x,y,z; the direction j is perpendicular to the interface).

[38] With $\Delta\mathbf{X}_1^*$ we denote the remaining dispersive displacement vector after the particle already performed the displacement $\Delta\mathbf{X}_1$ to reach the element interface (Figure 2). It can be calculated from,

$$\Delta X_{1,i}^* = \Delta X_{total,i}^* - \Delta X_{1,i}, \tag{15}$$

where $\Delta X_{total,i}^*$ is the total dispersive displacement calculated using the full time step Δt at the starting location of the particle with the random number vector ξ. $\Delta X_{1,i}^*$ and $\Delta X_{1,i}$ are related to the correct, nonlinearly split times Δt_1 and Δt_2, as

$$\Delta X_{1,i}^* = \Delta X_{1,i} \frac{\sqrt{\Delta t_2}}{\sqrt{\Delta t_1}}. \tag{16}$$

[39] For the direction i = j, the displacement in the second element, $\Delta X_{2,j}$, is calculated using a simple scaling according to equation (6),

$$\Delta X_{2,j} = \frac{\sqrt{D_{2(j,j)}}}{\sqrt{D_{1(j,j)}}} \Delta X_{1,j}^*, \tag{17}$$

where $\mathbf{D}_1$ and $\mathbf{D}_2$ are the dispersion tensors in the first and second element according to equation (2). Note that equation (17) describes a particle displacement away from the element interface into the second element which is consistent with the definition of the reflection coefficient.

[40] As stated above, the probability that a particle reaches the interface during Δt increases with higher values for the displacement in the direction j. As a consequence, the expected value of all displacements in direction j of all particles that reach the interface within time step Δt is larger than zero in the first, $E(\Delta X_{1,j}) > 0$, and second, $E(\Delta X_{2,j}) > 0$, element. Because of off-diagonal terms in the dispersion tensor $\mathbf{D}$ (equation (2)) that are different from zero, the displacements in the direction parallel to the interface are correlated to the displacements in the direction perpendicular to the interface; thus, $E(\Delta X_{1,i}) \neq 0$ and $E(\Delta X_{2,i}) \neq 0$. Because the direction of the flow vector and the dispersivities change across the interface, the off-diagonal terms in $\mathbf{D}$ and hence the correlation between the displacement in the direction perpendicular and parallel to the interface changes across the interface.

[41] To avoid a bias in the particle movements in the second element the correlation between the dispersive displacements parallel and perpendicular to the interface in the two elements must be accounted for appropriately. For any displacement, the expected value of the displacement in direction i, $\Delta X_{1,corr,i}$, that is conditioned on the displacement in direction j, $\Delta X_{1,j}$, is obtained as

$$\Delta X_{1,corr,i} = \frac{D_{1(i,j)}}{D_{1(j,j)}} \Delta X_{1,j}. \tag{18}$$

[42] Thus, the remaining correlated displacement $\Delta X_{1,corr,i}^*$ is

$$\Delta X_{1,corr,i}^* = \frac{D_{1(i,j)}}{D_{1(j,j)}} \Delta X_{1,j}^*. \tag{19}$$

[43] Similarly, $\Delta X_{2,corr,i}$ is the expected displacement in direction i in the second element that is conditioned on the displacement in direction j, and can be obtained as

$$\Delta X_{2,corr,i} = \frac{D_{2(i,j)}}{D_{2(j,j)}} \Delta X_{2,j}. \tag{20}$$

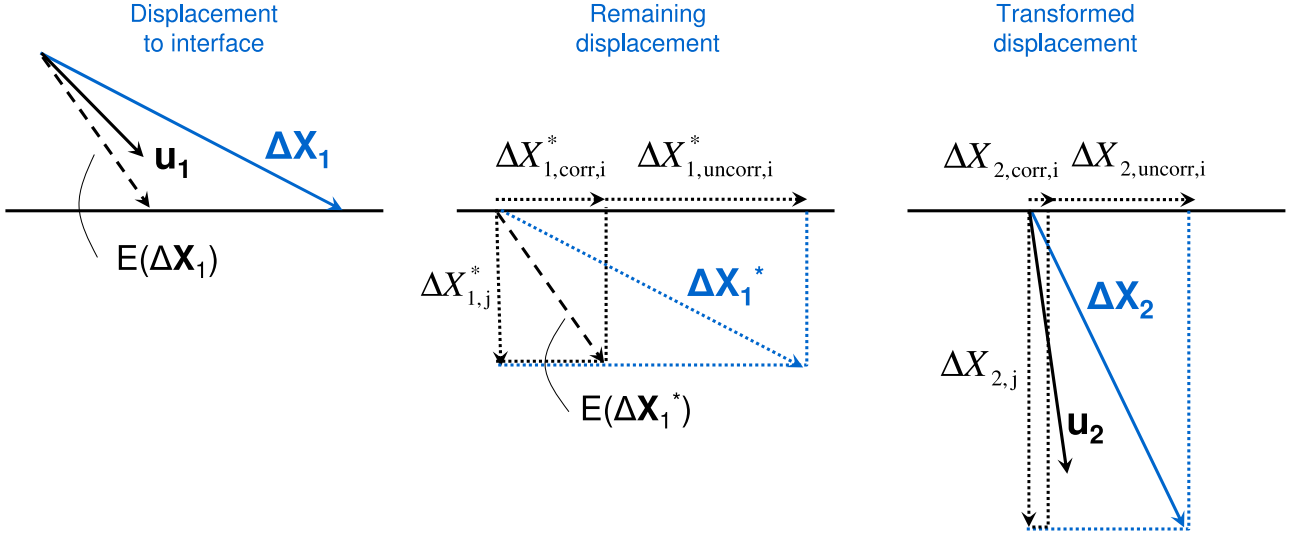

Figure 2. Transformation of dispersive displacement, schematically shown in two-dimensional for $\alpha_L > \alpha_T > 0$. (left) A particle performs the random dispersive displacement $\Delta\mathbf{X}_1$ and reaches the interface after $0.5\Delta t$. Note that the expected direction of dispersive displacements reaching the interface during a single Δt, $E(\Delta\mathbf{X}_1)$, is not parallel to the direction of the velocity $\mathbf{u}_1$. (middle) The remaining displacement based on the properties of the first element, $\Delta\mathbf{X}_1^*$, has a component perpendicular and components parallel to the interface. The latter can be split into a correlated and uncorrelated part. (right) The individual components of $\Delta\mathbf{X}_1^*$ are transferred to a dispersive displacement in the second element, $\Delta\mathbf{X}_2$, applying equations (15)–(24). For further details see section 2.2.3.

[44] Using equation (17), we obtain:

$$\Delta X_{2,\mathrm{corr,i}} = \frac{D_{2(\mathrm{i,j})}}{\sqrt{D_{2(\mathrm{j,j})}}\sqrt{D_{1(\mathrm{j,j})}}}\Delta X^*_{1,\mathrm{j}}. \tag{21}$$

[45] Note that for i = j, equation (21) simplifies to equation (17).

[46] After passing the correlated components, the uncorrelated components of the displacements in the different directions are transferred to the second element. The expected value of the uncorrelated displacement for i ≠ j is zero. The uncorrelated component, $\Delta X^*_{1,\mathrm{uncorr,i}}$, is the difference between the total remaining displacement in direction i and the displacement that is correlated to the displacement in direction j:

$$\Delta X^*_{1,\mathrm{uncorr,i}} = \Delta X^*_{1,\mathrm{i}} - \Delta X^*_{1,\mathrm{corr,i}}. \tag{22}$$

[47] As the uncorrelated displacement $\Delta X_{2,\mathrm{uncorr,i}}$ is only a part of the total displacement in direction i, the scaling from equation (17) has to be corrected for the already-treated correlated displacement. According to conditional statistics, $\Delta X^*_{1,\mathrm{uncorr,i}}$ is scaled by the ratio of the standard deviations of the uncorrelated displacements:

$$\Delta X_{2,\mathrm{uncorr,i}} = \Delta X^*_{1,\mathrm{uncorr,i}} \frac{\sqrt{D_{2(\mathrm{i,i})} - \left(\frac{D_{2(\mathrm{i,j})}}{\sqrt{D_{2(\mathrm{j,j})}}}\right)^2}}{\sqrt{D_{1(\mathrm{i,i})} - \left(\frac{D_{1(\mathrm{i,j})}}{\sqrt{D_{1(\mathrm{j,j})}}}\right)^2}}. \tag{23}$$

[48] For the direction j, it follows that $\Delta X_{2,\mathrm{uncorr,j}} = 0$. The displacement in direction i ≠ j in the second element is the sum of the correlated and uncorrelated displacement components,

$$\Delta X_{2,\mathrm{i}} = \Delta X_{2,\mathrm{corr,i}} + \Delta X_{2,\mathrm{uncorr,i}}. \tag{24}$$

[49] If the transport problem is one-dimensional or if $\mathbf{B}_2$ is linearly related to $\mathbf{B}_1$, the proposed transformation scheme coincides with a solution using the same set of random numbers for displacements in the first and second element and our new nonlinear time splitting with $\Delta\mathbf{X}_2 = \boldsymbol{\xi}\mathbf{B}_2\sqrt{\Delta t_2}$ (see equations (9) and (16)).

[50] When a particle is reflected at an interface or domain boundary, a point reflection at the interception point of displacement vector and interface must be performed (the whole remaining displacement vector is inverted). When reflecting solely the displacement component perpendicular to the interface (surface reflection), anisotropic dispersion tensors would be systematically distorted which leads to significant errors.

3. Materials and Methods

3.1. Numerical Implementation of the Improved Reflection Barrier Method

[51] For the calculation of the reflection coefficients the dispersion coefficients and water contents on both sides of the interface are necessary. In the case of anisotropic dispersion tensors, the component corresponding to the direction orthogonal to the interface has to be used, as it determines the probability that a particle reaches the interface. As our implementation was restricted to rectilinear grids we used the corresponding diagonal component of **D**. However, other choices are possible (e.g., a vector norm for the corresponding row vector of the dispersion tensor). For simulated flow field solutions, in which the velocity vector is continuously changing in space, it is important to calculate the reflection coefficient by taking the limits of the properties (velocity, dispersivity, diffusion coefficient, and water content) from both sides directly at the interface to guarantee that there is no reflection when the dispersion tensor and the water content is steady over the interface. Continuous changes of the dispersion tensor are considered already in the advective term of equation (3) and should not affect the value of the reflection coefficient.

[52] In previous studies, it has been reported that particles crossing different interfaces by dispersive displacements during the same time step Δt is a major problem for the application of the reflection barrier method to complex multidimensional transport problems [e.g., *LaBolle et al.*, 1996; *Salamon et al.*, 2006]. We used the simplest approach to treat particles that cross multiple interfaces during one time step. At each interface a particle reaches by dispersive movement, the reflection coefficient is calculated and a new random number is generated to decide whether the particle is reflected or allowed to pass. The subsequent dispersive displacement is then calculated on the basis of the proposed transformation of the dispersive displacement. Following this procedure the dispersive displacements are performed until the particle does not reach another interface within the remaining time. In this simple approach we do not superimpose multiple reflections to calculate the transition probability at a single interface, which has been considered to be the main reason for the problems with the application of the reflection barrier method to complex multidimensional scenarios. As will be demonstrated later, this works well as the proposed new transformation of the dispersive displacement allows a transfer of the remaining dispersive displacement from the first element to the second element at each interface without introducing a significant bias to the displacement in the second element.

[53] For the reflection barrier method in general, a splitting approach has to be used for the advective and dispersive displacements across discontinuities. First, the advective displacement is calculated with a linear time splitting $\Delta t = \Delta t_1 + \Delta t_2$, then the dispersive displacement is applied with the nonlinear time splitting $\sqrt{\Delta t} = \sqrt{\Delta t_1} + \sqrt{\Delta t_2}$ for scalar dispersion coefficients or the transformation of the dispersive displacement for dispersion tensors. The reflection principle must only be applied when a particle reaches an interface in the dispersion step.

[54] The different types of reflection coefficients and time splitting schemes, the transformation procedure of the dispersive displacement, and the interpolation method were implemented in the RWPT code PARTRACE [*Neuendorf*, 1997]. PARTRACE simulates three-dimensional transport of conservative and reactive solutes in saturated and unsaturated porous media for given velocity fields by applying the stochastic differential equation given in equation (3) to a high number of particles. The dispersive displacement matrix **B** of equation (3) is calculated as given in equation

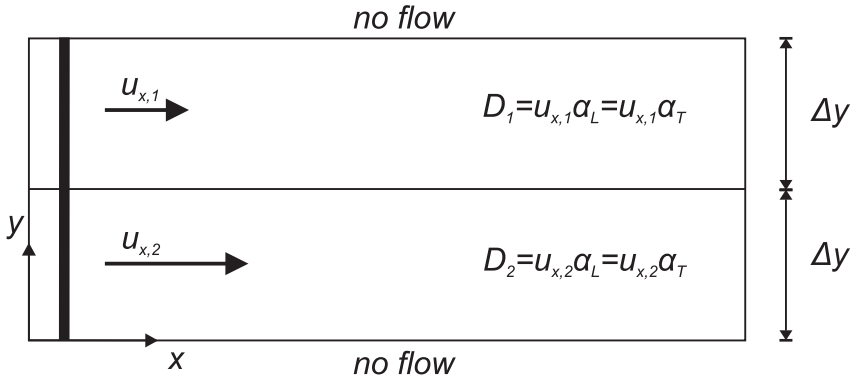

Figure 3. Schematic overview of scenario S1 which was adopted from *Salamon et al.* [2006]. Details and parameters are presented in the scenario description.

(4). PARTRACE is a modular c++ code, capable of handling regular and irregular grids, and parallelized for use on massive parallel supercomputers.

3.2. Numerical Verification of the Improved Reflection Barrier Method

[55] To verify the three improvements of the proposed RWPT algorithm, we performed numerical simulations of conservative solute transport in specific test scenarios. Two different test scenarios are considered. The first scenario, S1, is a simplified transport problem for which an analytical solution exists (for a schematic view of the test scenario see Figure 3). For this test scenario a basic version of the proposed algorithm can be used that only uses the first two improvements (nonlinear time splitting and one-sided reflection scheme). Although this test case seems very simple, it is absolutely essential, as it is not possible to clearly differentiate between the effects of the individual improvements in complex three-dimensional test cases.

[56] In the second scenario, S2, we applied the improved reflection barrier method to a complex three-dimensional, unsaturated transport problem based on a computed velocity field and compared the results with the ones obtained from the interpolation method, abbreviated by I (Figure 4 and Table 1). We used a material distribution created by a sequential indicator algorithm, which is the most demanding type of parameter heterogeneity for RWPT algorithms according to *Salamon et al.* [2006]. The finite volume or finite difference solution of the water flow problem computed for such a scenario is characterized by many abrupt changes of the dispersion tensor and of the water contents that occur at element interfaces.

[57] All scenarios were simulated using the two different reflection coefficients, R1 and R2 (see Figure 1), and using the linear, TS1 as well as the corrected time splitting, TS2. Scenario S2, where a transformation of the dispersive displacement is required, was additionally simulated without (DT0), i.e., $\Delta\mathbf{X}_2 = \boldsymbol{\xi}\mathbf{B}_2\sqrt{\Delta t_2}$, and with (DT1) performing the proposed dispersive displacement transformation (for an overview of options see Table 1).

[58] The amount of particles used are indicated for each scenario and were chosen to minimize the fluctuations of the solution to an acceptably low value while obtaining a computational speed high enough for a spatial and temporal convergence analysis on the available computation cluster. For scenario S2 an analysis of the convergence as function of the particle number was performed as well.

4. Test Scenarios

4.1. Test Scenario S1

4.1.1. Problem Description

[59] This two-dimensional scenario of transport in a two-layer stratified aquifer was adopted from *Salamon et al.*

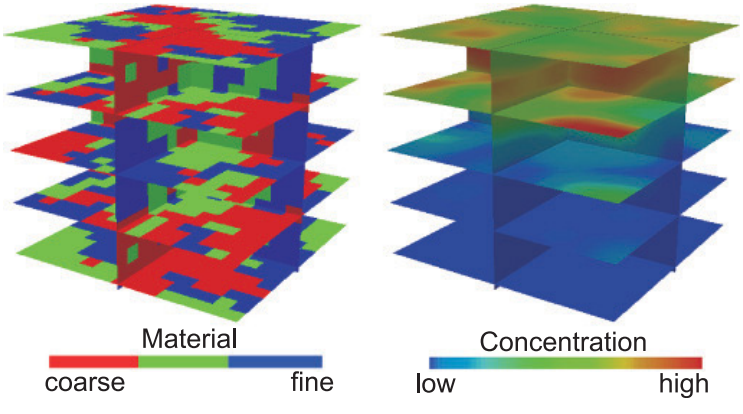

Figure 4. (left) Trimodal correlated indicator field used as hydraulic parameter field for scenario S2. (right) Solute distribution of scenario S2–1 at time $t = 17$ d after a Dirac pulse tracer injection at the soil surface under infiltration conditions.

Table 1. Overview of Options of the Reflection Barrier Method Applied to the Scenarios S1 and S2

	Option	Abbreviation
	Reflection Coefficient	
Lim [2006]	Two-sided	R1
This study	One-sided	R2
	Time Splitting	
Hoteit et al. [2002]	$\Delta t = \Delta t_1 + \Delta t_2$	TS1
This study	$\sqrt{\Delta t} = \sqrt{\Delta t_1} + \sqrt{\Delta t_2}$	TS2
	Transformation of Dispersive Displacement	
Hoteit et al. [2002]	No transformation applied	DT0
This study	Transformation applied, equations (15)–(24)	DT1

[2006]. Using this scenario, they compared the interpolation, GSDE, and reflection barrier methods. The results indicated significant discrepancies between the methods and the analytical solutions for this test scenario, which are given by *Marle et al.* [1967]. We kept the settings as presented by *Salamon et al.* [2006] to maintain comparability with their results (see also Figure 3 for a schematic overview). The domain size was 10,000 m in the x-direction (horizontal) and 0.3 m in the y-direction (vertical) with a regular discretization of 100 × 30 elements and reflection boundary conditions at the top and bottom domain boundary. The extreme x/y ratio was chosen by Salamon et al. to highlight the differences between the methods. Both layers had a thickness of 0.15 m and a porosity of $\theta = 0.2$. Steady state water flow was horizontal from left to right. The velocity in the lower layer was $u_{x2} = 43.2$ m d^{-1}, and the velocity in the upper layer, u_{x1}, ranged in different scenarios from 43.2 m d^{-1} to 0.043 m d^{-1} covering ratios u_{x2}/u_{x1} between 1 and 1000. The dispersion in the layers was assumed to be isotropic and the dispersion coefficient was calculated from the pore water velocity using $D = \alpha\, u$, with α being the dispersivity (0.01 m). A Dirac pulse was uniformly injected in the y-direction at time $t = 0$ d (6×10^3 particles), sufficiently far away from the left domain boundary to assure that no particles would be affected by the left boundary condition. We analyzed the transport results by applying the method of moments [*Aris*, 1956] as done by *Salamon et al.* [2006]. The first three spatial moments were calculated for the x-direction directly from the particle locations by the equations:

$$M_0(t) = nm, \tag{25}$$

$$M_x(t) = \frac{m}{M_0(t)} \sum_{i=1}^{n} x_i(t), \tag{26}$$

$$M_{xx}(t) = \frac{m}{M_0(t)} \sum_{i=1}^{n} x_i^2(t) - M_x^2(t), \tag{27}$$

where n is the number of particles, m is the particle mass, and $x_i(t)$ is the position of the particle i in the x-direction at time t. M_0 represents the total solute mass (kg), M_x represents the position of the center of mass in the x-direction (L), and M_{xx} represents the spreading of the plume in the x-direction (L^2). The location of the center of mass and the plume spreading in the y-direction are obtained by replacing the x- by the y-coordinate in the equations above.

[60] The apparent average velocity $U(t)$ and the apparent longitudinal macrodispersion $D_L(t)$ can be derived from the moments:

$$U_x(t) = \frac{M_x(t) - M_x(0)}{t}, \tag{28}$$

$$D_L(t) = \frac{1}{2}\frac{M_{xx}(t) - M_{xx}(0)}{t}. \tag{29}$$

[61] Numerical results of the location of the center of mass in the y-direction and longitudinal macrodispersion $D_L(\mathrm{t} \rightarrow \infty)$ were compared with analytical solutions [*Marle et al.*, 1967]. The only differences to the simulations of *Salamon et al.* [2006] is that we extended the domain in the x-direction from 1000 to 10,000 m and that we calculated the longitudinal macrodispersion for $t = 200$ d. The reason for these modifications is that the spatial and time dimensions used by *Salamon et al.* [2006] were not sufficient to assume $D_L(\mathrm{t} \rightarrow \infty)$ for the most extreme scenario with the velocity ratio $u_{x2}/u_{x1} = 1000$.

4.1.2. Results and Discussion

[62] Existing reflection schemes can lead to deviations between numerical results and analytical solutions in well-defined test scenarios [*Salamon et al.*, 2006]. Our results for test scenario S1 demonstrate that the corrected time splitting already corrects for part of these deviations (Figure 5a). We reproduced similar deviations as observed in *Salamon et al.* [2006] by applying the wrong time splitting and the two-sided reflection scheme which shifted the center of mass in the y-direction to the low dispersion layer.

[63] The application of the corrected time splitting TS2 is sufficient to predict the center of mass in the y-direction correctly; however, the spreading in the x-direction, i.e., the longitudinal macrodispersion, is not accurately simulated for higher Δt when applying TS2 in combination with the two-sided reflection scheme R1. Redundant reflections in the two-sided reflection scheme cause two errors: (1) they decrease the exchange between the two layers and (2) cause a retarded transversal spreading of the particles entered in layer 1 or 2. Both biases affect the accuracy of the longitudinal dispersion (Figure 5b). Our improved one-sided reflection scheme R2 also provided very accurate results for large time steps as the error related to the reflection barrier method was then limited to a reduced number of particle reflections at the single material contrast between layer 1 and 2 (Figure 5b). The results that are obtained even with large time steps when using the corrected time splitting TS2 and the one-sided reflection scheme R2 are fully consistent with the analytical solution and more accurate than all results presented in the comparative study of *Salamon et al.* [2006] for this test scenario with the interpolation, the GSDE, the reflection, and the total variation diminishing (TVD) scheme.

4.2. Test Scenarios S2–1 and S2–2

4.2.1. Problem Description

[64] The scenarios S2–1 and S2–2 were chosen to demonstrate the general applicability of the improved reflection barrier method to more complex three-dimensional transport

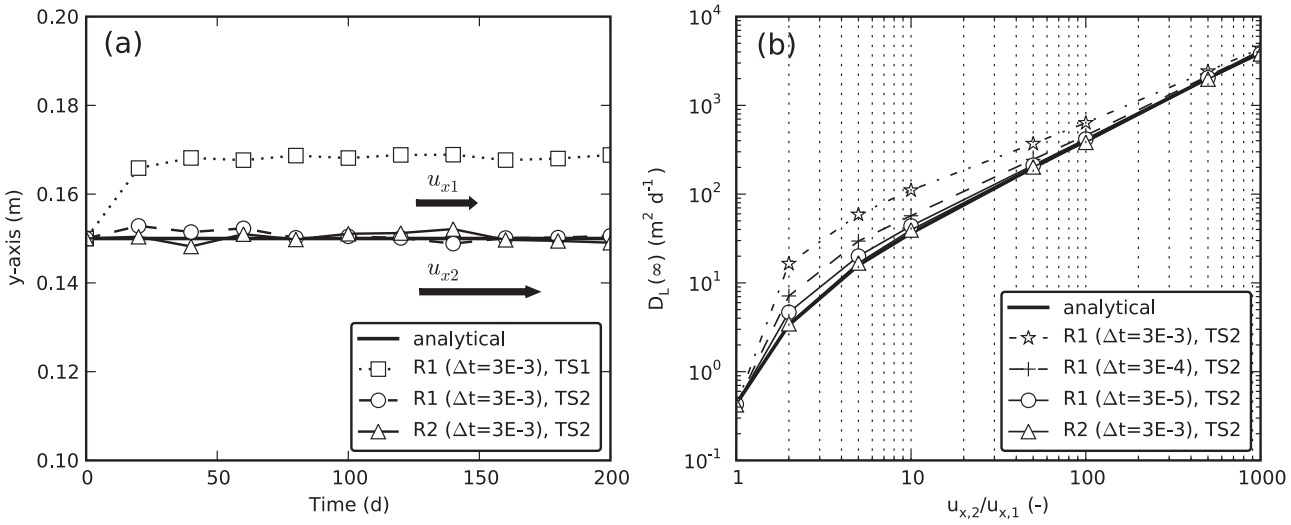

Figure 5. Scenario S1. (a) Location of the center of mass in the y-direction (m) versus time (d) for $u_{x2}/u_{x1} = 1000$. (b) Longitudinal macrodispersion $D_L(t \rightarrow \infty)$ as a function of increasing heterogeneity u_{x2}/u_{x1}. Reflection coefficients R1: [*Lim*, 2006] and R2: one-sided reflection scheme; time splitting TS1: $\Delta t = \Delta t_1 + \Delta t_2$ and TS2: $\sqrt{\Delta t} = \sqrt{\Delta t_1} + \sqrt{\Delta t_2}$.

problems. In these scenarios, the RWPT algorithm has to deal with complexities such as: (1) a heterogeneous flow field, (2) a continuously and discontinuously spatially changing anisotropic dispersion tensor, (3) eigenvectors of **D** oriented oblique to the interface, (4) spatially varying water content, and (5) multiple reflections during a single time step Δt. To analyze whether our proposed improvements to the reflection barrier method, i.e., the corrected time splitting TS2 and the one-sided reflection scheme R2, also lead to improvements in complex problems, the transport of a tracer pulse was considered (scenario S2–l). In the scenarios S2–l and S2–2, we further analyzed how the transformation of the dispersive displacement improves the accuracy of the results.

[65] The water flow and the water content were simulated for a constant flux boundary condition of 10^{-3} m d^{-1} at the top surface of a three-dimensional heterogeneous unsaturated porous medium. The porous medium corresponds to an experimental setup at the Agrosphere Institute in Jülich that consists of a 0.875 m × 0.875 m × 0.8317 m heterogeneously filled sank tank. The tank was filled with rectangular blocks (15 × 15 × 14 blocks, see Figure 4) of three different sandy materials (here called fine-, medium-, and coarse-grained; the hydraulic properties are given in Table 2). To analyze how the efficiency of the algorithm depends on the variance of the hydraulic parameter field, we created two additional hydraulic parameter sets for the scenarios S2–l and S2–2 with a lower and a higher variability applying the concept of Miller-similarity scaling [*Miller and Miller*, 1956]. The hydraulic parameters with the lower variability were obtained by dividing the saturated conductivity K_s and the van Genuchten-Mualem parameter α of the coarse material by 3 and $\sqrt{3}$, respectively, and multiplying K_s and α of the fine material by 3 and $\sqrt{3}$, respectively. The hydraulic parameters with the higher variability were obtained by multiplying K_s and α of the coarse material by 3 and $\sqrt{3}$, respectively, and dividing K_s and α of the fine material by 3 and $\sqrt{3}$, respectively. The variances of $\ln(K_s)$ of the three resulting parameter fields are 0.88, 4.2, and 21.2 and the variances of the water content θ are 0.0018, 0.006, and 0.013. We will further refer to them as low, intermediate, and high parameter variability.

Table 2. Van Genuchten-Mualem Parameters of Materials in S2[a]

	θ_r (m^3 m^{-3})	θ_s (m^3 m^{-3})	α (cm^{-1})	n (−)	K_s (cm d^{-1})	λ (−)
Coarse	0.05	0.41	0.0177	10.8	2496	0.73
Medium	0.06	0.36	0.0121	5.3	408	−0.01
Fine	0.07	0.35	0.0055	3.5	48	0.66

[a]θ_r = residual water content; θ_s = saturated water content; K_s = saturated conductivity; α, n and λ = shape parameters.

[66] The arrangement of the blocks was generated using an indicator random field generator SISIM, which is part of the Geostatistical Software Library (GSLIB) [*Deutsch and Journel*, 1998]. The 1.5 cm bottom layer is composed of the fine material only. The lower boundary condition was a constant pressure of −2.5 hPa. No-flow boundary conditions were used at the sides of the tank. The flow field was simulated using Richards' equation. The equation was solved using a cell-centered finite-volume (FV) scheme on rectilinear grids with full-upwinding of relative permeability in space for stabilization. An implicit Euler scheme was used for the time discretization. Linearization of the nonlinear equations is done by an inexact Newton method with line search. The linear equations are solved with an algebraic multigrid solver. The time step is automatically adapted by the time solver. The flow field was interpolated using RT0 Raviart Thomas elements [*Brezzi and Fortin*, 1991; *Raviart and Thomas*, 1975]. The numerical code was tested with analytical solutions and successfully applied in several studies [*Bechtold et al.*, 2011; *Haber-Pohlmeier et al.*, 2010; *Ippisch et al.*, 2006; *Rossi et al.*, 2008; *Samouelian et al.*, 2007].

[67] Differences between the hydraulic properties of the sand blocks led to a highly heterogeneous flow field and large water content variations in the soil profile ranging

from 0.06 to 0.41. In both scenarios S2–1 and S2–2, an anisotropic dispersion tensor was defined. The longitudinal and transversal dispersivities were set to 0.1 and 0.02 m, respectively, for all three materials and the molecular diffusion coefficient was assumed to be zero.

[68] In scenario S2–1 a Dirac pulse (1×10^6 particles) was injected at $t = 0$ d at the soil surface into the simulated steady state flow field. Both the concentration of the irrigated water and the initial concentration of pore water before the injection were 0 kg m^{-3}. In S2–1, we compared the spatial moments of the concentration distributions (Figure 4, equations (25)–(29)) obtained with the different particle-tracking methods.

[69] Scenario S2–2 served as a test whether the improved reflection barrier method is able to maintain constant concentration in such a transport problem when the system is continuously flushed with the same concentration. The initial concentration was set to $C_0 = 1$ kg m^{-3}, i.e., particles were heterogeneously injected depending on the water content (in total 7.5×10^6 particles, each having a mass of $\sim 2.7 \times 10^{-8}$ kg). The concentration of the irrigated water also had a concentration of $C = 1$ kg m^{-3}, to maintain the amount of particles necessary to preserve a constant and homogeneous concentration of $C(\mathbf{X},t) = 1$ kg m^{-3}. As a performance measure, we compared the simulated concentrations of the $15 \times 15 \times 15$ elements each representing a material block with the true, constant concentration of 1 kg m^{-3} by calculating the RMSE of all elements,

$$\mathrm{RMSE} = \sqrt{\frac{\sum_i \left(C_i(\mathbf{X},t) - C_0\right)^2}{n_{elements}}}. \tag{30}$$

[70] The RMSE error was calculated at $t = 10$ d when the RMSE error reached a steady state in all cases. As a reference, we calculated the RMSE that can be expected from a RWPT simulation with the applied number of particles. In this calculation, we assumed that the particles were randomly distributed over the domain elements so that the concentration is uniform. Thereby, the probability that a particle is placed in a specific element depends on the volume and water content of this element (for details see Appendix A).

[71] The interpolation method was implemented using the "hybrid" scheme described above [*LaBolle et al.*, 1996]. The improved reflection barrier method was compared with the interpolation method by performing a spatial and temporal convergence analysis. As stated above, RWPT is principally a grid-free method; however, grids are needed to represent the spatial variation of the variables governing the particle motion (here velocity, dispersion tensor, and water content) and calculate these variables at the particle location by interpolation. The input to all RWPT simulations was the steady state flow field computed on the coarsest grid ($15 \times 15 \times 15$ elements). Different grids were then applied in the RWPT algorithm to interpolate the variables. The coarsest grid we used for the RWPT simulations was equal to the one of the flow solution and consisted of $15 \times 15 \times 15$ elements (3375 elements), each element representing one material cube (including the homogeneous bottom layer). For the spatial convergence analysis, the grid was gradually refined by doubling the number of elements in each direction during one refinement step. In the following, we refer to the different refined grids with the refinement factor k, which is the number of subdivisions along each axis of the element of the coarsest grid. The finest grid consisted of $120 \times 120 \times 120$ elements (1.7×10^6 elements, grid refinement factor, $k = 8$). The particle positions obtained from the RWPT simulations were always used to map the solute concentration to the coarsest grid, so that all results were compared at the same resolution. For the temporal convergence analysis, we applied time step sizes ranging from $\Delta t = 0.001$ to 1.0 d. To focus on the accuracy of the dispersive displacements in the temporal convergence analysis, we minimized the effect of different time step sizes on the calculation of the advective term of equation (3) by implementing the analytical velocity integration after *Pollock* [1988] and *Schafer-Perini and Wilson* [1991], which is exact for a linearly varying velocity field as provided by the FV solution. Here for simplicity only written for the x-direction:

$$x - x_0 = \frac{a + b(x_1 - x_0)}{b} \exp(b\Delta t) - \frac{a}{b} \tag{31}$$

using the velocity interpolator within one element from the FV solution,

$$u_{x,1} = a + b(x_1 - x_0), \tag{32}$$

where x is the new particle location after time Δt, x_1 is the initial particle location, x_0 is the coordinate of the left side of the element, a and b are variables of the velocity interpolation using RT0 Raviart Thomas elements, and $u_{x,1}$ is the velocity at the initial particle coordinates x_1. The velocity of a particle that leaves the element during Δt was updated at the interception point, the time was split linearly $\Delta t = \Delta t_1 + \Delta t_2$, and the second displacement was performed with the updated velocity and the remaining time Δt_2.

4.2.2. Results and Discussion

[72] Simulations from applying different combinations of options for the reflection barrier method were compared for S2–1 and the intermediate parameter variability (Figure 6). The results indicate that all methods converge to similar calculated first and second moments with decreasing time step size. The use of a two-sided reflection scheme R1 leads to a higher apparent average velocity and a smaller longitudinal macrodispersion compared to the one-sided reflection scheme R2, especially for larger time steps. The linear time splitting scheme TS1 results in a lower apparent average velocity and a higher longitudinal macrodispersion than the nonlinear time splitting scheme TS2, also more pronounced for larger time steps. The largest initial deviations occurred when applying both R1 and TS1. When the two-sided reflection scheme R1 was used with the correct time splitting TS2, the trend is the same, the observed errors were a bit lower but the effects did not completely compensate. The best results with large time steps and the fastest convergence were obtained when both improvements, R2 and TS2 were applied. The application of the transformation of the dispersive displacement, in the following called DT1, shifted the apparent average velocity to higher values compared to the combination of R2 and TS2, the apparent longitudinal macrodispersion was almost identical, and convergence was even faster.

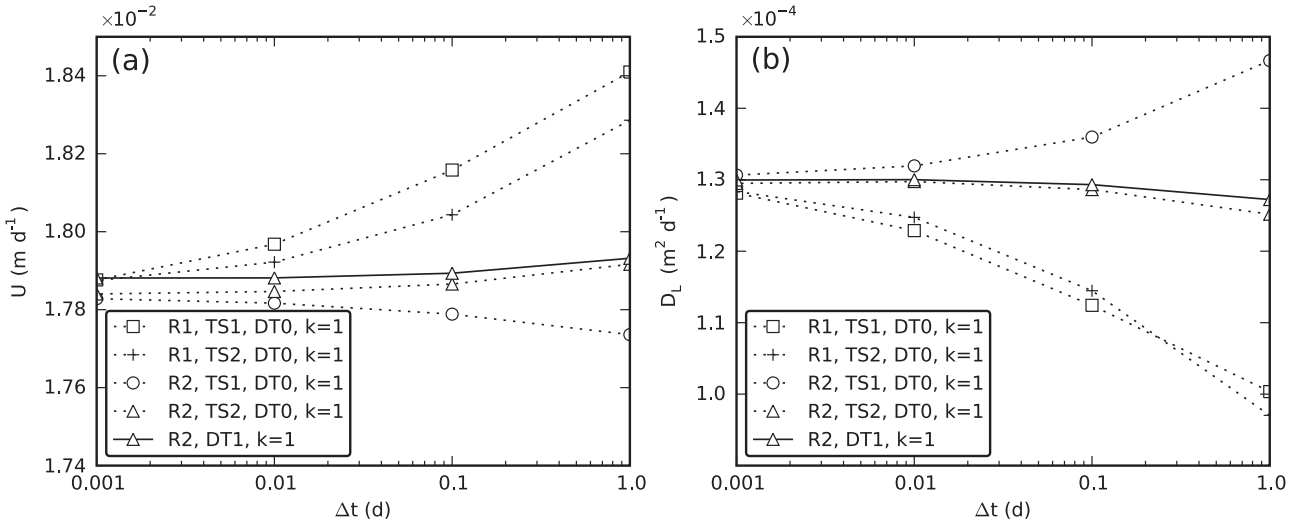

Figure 6. (a) Scenario S2–l, apparent average velocity U, and (b) apparent longitudinal dispersion D_L, as a function of applied time step size for the coarsest grid (no grid refinement, refinement factor $k = 1$) at time $t = 17$ d. Reflection coefficients R1: [*Lim*, 2006] and R2: one-sided reflection scheme; time splitting TS1: $\Delta t = \Delta t_1 + \Delta t_2$ and TS2: $\sqrt{\Delta t} = \sqrt{\Delta t_1} + \sqrt{\Delta t_2}$; transformation of dispersive displacement DT0: not applied, DT1: applied, no time splitting necessary.

[73] To evaluate the accuracy of these results, a comparison with a reference numerical method, the interpolation method was performed. There is general agreement that the interpolation method converges to the true solution when refining the grid and the time step size simultaneously. The comparison between the improved reflection barrier and the interpolation method served to evaluate whether the results of the improved reflection barrier method are also reliable for complex three-dimensional transport problems. This comparison was performed for all three parameter fields.

[74] Figure 7 shows that the results of the apparent average velocity and the apparent longitudinal macrodispersion obtained from the interpolation method converged for the low and intermediate parameter variability when simultaneously decreasing the grid size and time step. In these cases, the interpolation method converged to a solution that is consistent with the solution to which the reflection barrier method was converging when applying R2 and DT1. By neglecting the transformation of the dispersive displacement (option DT0), the reflection barrier method did not converge to the same solution. This demonstrates the improvement achieved by the transformation of the dispersive displacement. The improved reflection barrier method was practically independent of the grid size (Figure 7). For the highest parameter variability, the interpolation method apparently did not converge with the finest grid and smallest time step size, in contrast to the reflection barrier method. The results of the interpolation method indicate that a further grid refinement and time step size reduction probably provides results that approach the ones of the reflection barrier method. However, because of memory issues, a further grid refinement could not be performed.

[75] In the last scenario S2–2, it was tested how the improved reflection and interpolation method can maintain a homogenous concentration in a steady state flux field with advective and dispersive transport. S2–2 represents a classical scenario for which an accumulation of solute in low dispersive regions occurs when a standard RWPT scheme is applied, which neglects discontinuities of **D** and θ are not accounted for [*Hoteit et al.*, 2002]. We first focus on the results of the intermediate parameter variability. Figure 8 (left) illustrates the high error when neglecting the effect of discontinuous dispersion tensors and applying neither the interpolation nor the improved reflection barrier method ("standard RWPT"). The calculated root-mean-square error (RMSE, see equation (30)) between the simulated concentration and the uniform background concentration ($C = 1$ kg m^{-3}) was 0.77 for the smallest time step. The interpolation method applied on the coarse grid partly corrected these errors (compare Figure 9b), however, especially in the zone where high abrupt water content changes occur, the method has severe problems to maintain the homogenous concentration (RMSE = 0.29 for $\Delta t = 0.001$, Figure 8). For the finest grid, the interpolation method provided acceptable results (RMSE = 0.06 for $\Delta t = 0.001$). The improved reflection barrier provided good results for the coarsest and finest grid (RMSE = 0.03 for $\Delta t = 0.001$), even for the highest time step $\Delta t = 1.0$ (RMSE = 0.06). Only the improved reflection barrier method including DT1 converged to the reference RMSE that could be expected from the applied number of particles (see Appendix A). Both scenarios S2–l and S2–2 demonstrated that the transformation of the dispersive displacement is required for a proper convergence of the reflection barrier method.

[76] The results of the lower and higher parameter variability (Figures 9a and 9c) show that the RMSE error of both the interpolation and reflection barrier method generally increase with increasing parameter variability. However, the reflection barrier method is much less affected by higher parameter variability than the interpolation method. For the highest parameter variability, both the grid refinement and the time step reduction are far from sufficient for the interpolation method to converge to a final solution. In contrast, for

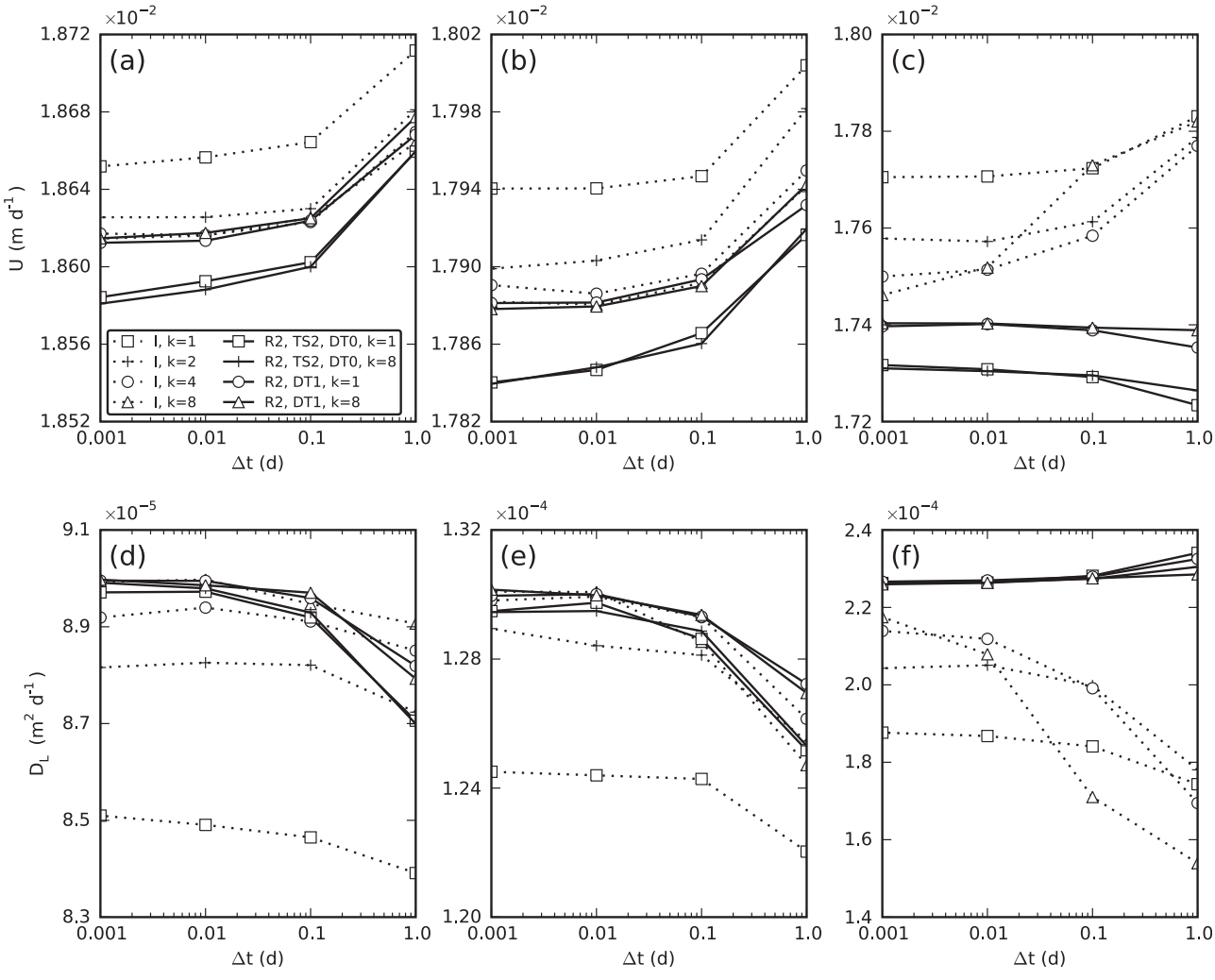

Figure 7. Scenario S2–1, (top) apparent average velocity U, and (bottom) apparent longitudinal dispersion D_L, as a function of applied time step size for different grid refinements (refinement factor $k = 1$–8, k is the number of subdivisions along each axis of the element of the coarsest grid) and different parameter variabilities (low: (a and d), intermediate: (b and e), high: (c and f)) at time $t = 17$ d. R2: one-sided reflection scheme, and I: interpolation method; time splitting for reflection barrier method TS2: $\sqrt{\Delta t} = \sqrt{\Delta t_1} + \sqrt{\Delta t_2}$; transformation of dispersive displacement DT0: not applied, DT1: applied, no time splitting necessary.

the lowest parameter variability, the interpolation method almost converged exactly to the reference RMSE.

[77] The dependency of the solution on the number of particles was evaluated for scenario S2–1 with the intermediate parameter variability, for which both the interpolation and the reflection barrier method converged to the same solution for $\Delta t = 0.001$. Ten model runs ($n_{\text{runs}} = 10$) were performed for each of three different numbers of particles ($n = 10^6$, 10^5, 10^4). We then calculated the normalized RMSE of the bulk concentration (mass per unit volume) C_b for the same time at which the apparent velocity and macrodispersion was evaluated before ($t = 17$ d),

$$\text{RMSE}_{\text{normalized}} = \sqrt{\frac{1}{n_{elements}} \sum_i \frac{1}{n_{\text{runs}}} \sum_j \left(\frac{C_{b(i,j)}(\mathbf{X}, t)}{\bar{C}_{b(i)}(\mathbf{X}, t)} - 1 \right)^2}, \tag{33}$$

where $\bar{C}_{b(i)}$ is the mean concentration of the solution at element i. Figure 10 shows the $\text{RMSE}_{\text{normalized}}$ as a function of the number of applied particles n_{par} for three different bulk concentration ranges. Within a concentration range, the fluctuations of the results of the interpolation and the reflection barrier method depend linearly on the inverse of the square root of the number of particles. Figure 10 further shows that for a specific number of particles, the magnitude of the fluctuations depends on the local concentration, with higher fluctuations where the concentrations are lower. This is the expected behavior for random walk particle tracking algorithms [*Kinzelbach and Uffink*, 1991].

[78] We also tested if a random vector $\mathbf{Z}$ with a uniform distribution between -1 and 1 can be used instead of the normally distributed random vector $\boldsymbol{\xi}$. However, we found that the transformation of the dispersive displacement is only consistently applicable when using the normally distributed random vector $\boldsymbol{\xi}$. The results from the application

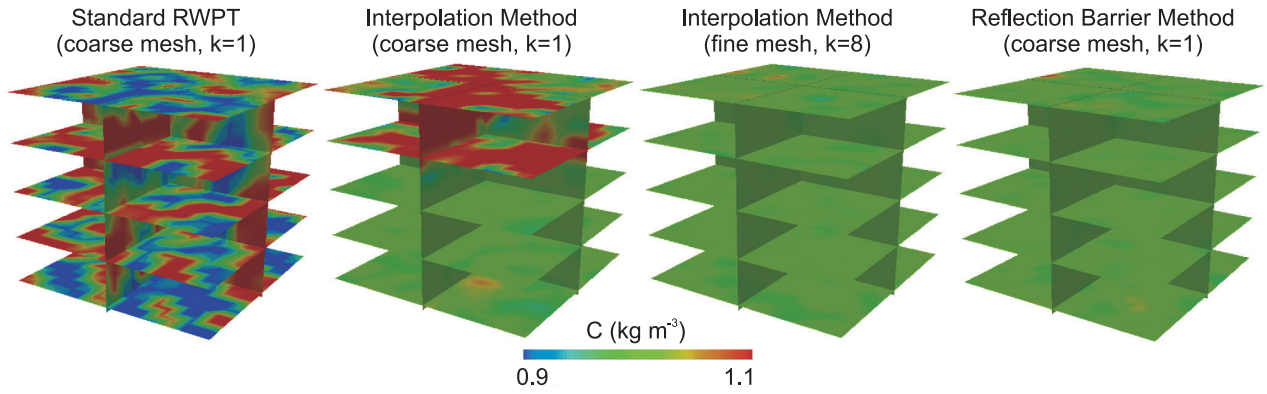

Figure 8. Scenario S2–2, constant concentration test. Shown are the solute concentrations at $t = 10$ d. In this scenario, C is ideally supposed to be homogenously and constantly 1 kg m^{-3}. RMSE error from left to right: 0.79, 0.29, 0.06, 0.03. All scenarios were calculated with the smallest time step size $\Delta t = 0.001$. Refinement factor $k = 1$, 2, 4 and 8, k is the number of subdivisions along each axis of the element of the coarsest grid. The reflection barrier method was applied using the corrected time splitting TS2, the one-sided reflection scheme R2, and the transformation of the dispersive displacement DT1.

of the uniformly distributed and from the normally distributed random vector differ in terms of their mean direction of the dispersive displacements that reach the interface ($E[\Delta \mathbf{X}_1]$ of Figure 2). Particularly, when using $\mathbf{Z}$ a mean dispersive displacement direction was obtained that differs from the expected correlated part of the dispersive displacement, which is in contrast to the theory of the proposed transformation of the dispersive displacement. Although the observed errors were very small in practical applications, we suggest the use of the normally distributed random vector $\boldsymbol{\xi}$ when applying the transformation of the dispersive displacement.

[79] Finally, the effect of neglecting water content variations were analyzed. For scenario S2–1 with intermediate parameter variability, simulations were performed using the reflection coefficient of *Hoteit et al.* [2002] which does not account for water content variations. Based on the results above, we used the proposed improved reflection scheme (R2, DT1) and the interpolation method with the finest grid size (I, $k = 8$) as reference for the true solution. Figure 11 shows the large deviations that occur when water content variations are not considered in the reflection coefficient.

[80] This test demonstrates the important improvement proposed by *Lim* [2006] when applying the reflection barrier method to porous media with varying porosity or water contents.

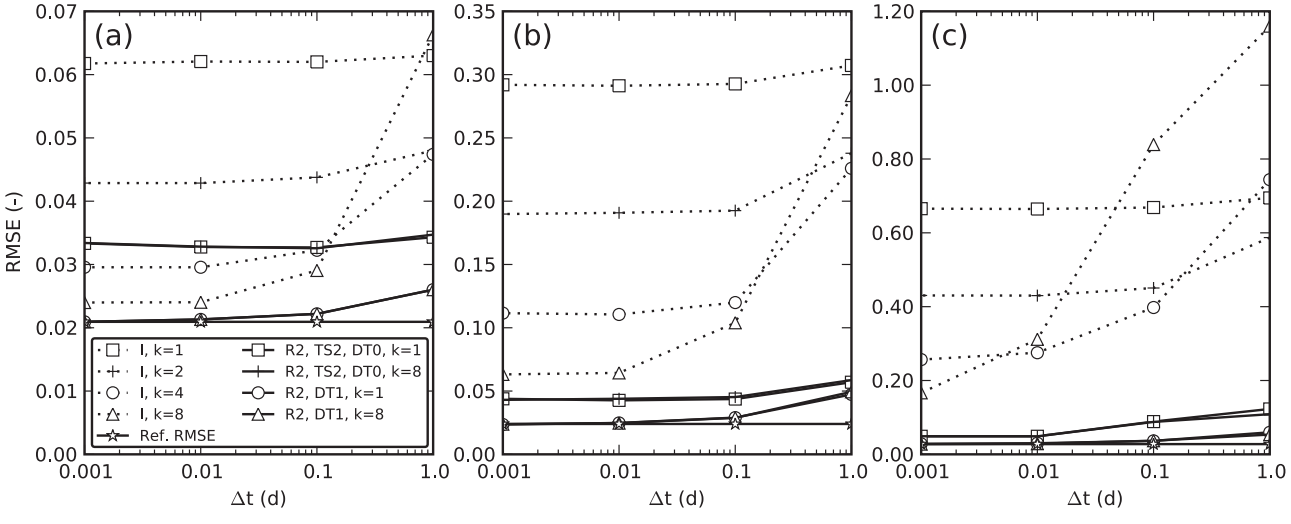

Figure 9. Scenario S2–2, RMSE at time $t = 10$ d of modeled and theoretical concentration $C = 1$ kg m^{-3} calculated from all elements as a function of applied time step size for different grid refinements (refinement factor $k = 1$, 2, 4 and 8, k is the number of subdivisions along each axis of the element of the coarsest grid) and different parameter variability ((a) low, (b) intermediate, (c) high). R2: one-sided reflection scheme, and I: interpolation method; time splitting for reflection barrier method TS2: $\sqrt{\Delta t} = \sqrt{\Delta t_1} + \sqrt{\Delta t_2}$; transformation of dispersive displacement DT0: not applied, DT1: applied, no time splitting necessary.

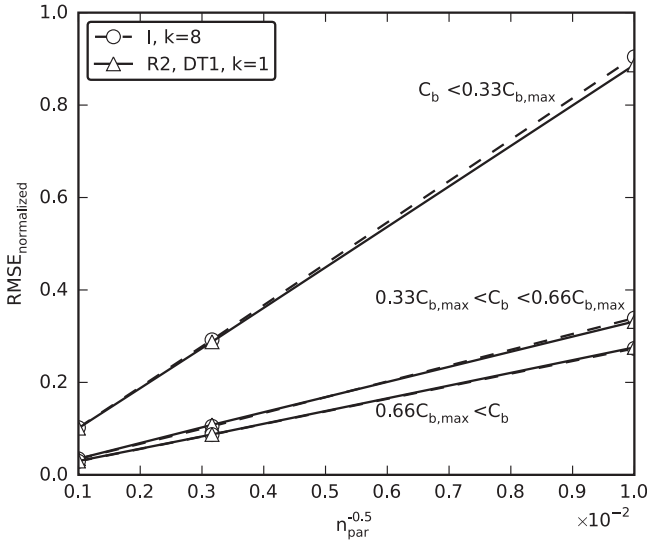

Figure 10. Convergence with the number of particles for scenario S2–l and intermediate parameter variability. Normalized RMSE as a function of the inverse of the root of the number of particles for three different bulk concentration ranges, where $C_{b,\max}$ is the maximum bulk concentration of the spatial concentration distribution of the true solution. I: Interpolation method, R2: one-sided reflection; DT1: transformation of dispersive displacement applied, no time splitting necessary; k: number of subdivisions along each axis of the element of the coarsest grid.

5. Discussion

5.1. Convergence to the True Solution

[81] In general, RWPT converges with the number of particles, the time step size, and in case of the interpolation method also with the resolution of the interpolation grid. The reflection barrier method is independent of the interpolation grid size. Velocity and water content are directly obtained by linear interpolation from the numerical flow solution. The interpolation method introduces an additional error by the interpolation of discontinuities as described in section 2.1. Convergence to the true solution is obtained by a simultaneous refinement of the interpolation grid and a reduction of the time step [*LaBolle et al.*, 1996; *Salamon et al.*, 2006].

[82] The results of both S2–l and S2–2 are completely consistent with this general behavior. For example, in S2–2 (at intermediate parameter variability) the interpolation method apparently performs poorly because the grid is still not fine enough. Even for the finest grid, a further decrease of the time step size would not lead to any improvement, as the solution already converged to the best solution for this level of refinement. Because of memory limits, a further refinement of the interpolation grid was not possible in this demanding three-dimensional scenario. For the reflection barrier method there is no change with grid refinement and the convergence to the correct solution with time step reduction is much faster when a transformation of the dispersive displacements and a one-sided reflection scheme were used.

5.2. Efficiency Considerations

[83] When comparing the results from the improved and the original reflection barrier method, the higher efficiency of the improved scheme is apparent in the more accurate results for the same time step Δt (see Figures 5–9). As the computation costs for the reflection barrier method and the interpolation method differ, the time step Δt cannot be taken directly as an indicator for the computational efficiency. We therefore evaluated the numerical error as a function of CPU time. For scenarios S2–l and S2–2 with the intermediate parameter field variance we calculated a

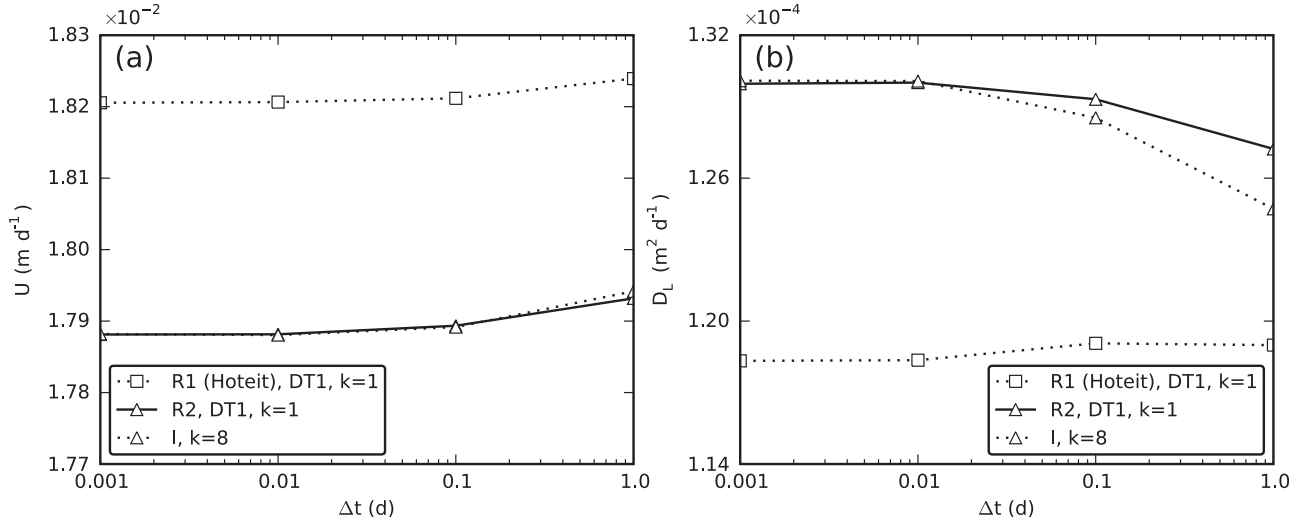

Figure 11. (a) Scenario S2–l, apparent average velocity U, and (b) apparent longitudinal dispersion D_L, at time $t = 17$ d as a function of applied time step size. Reflection coefficient R1: [*Lim*, 2006], here with the neglecting of water content variations which corresponds to the reflection coefficient of *Hoteit et al.* [2002], R2: one-sided reflection scheme (this study), and I: interpolation method; transformation of dispersive displacement applied (DT1), k: number of subdivisions along each axis of the element of the coarsest grid.

relative error which characterizes each result, ϑ_i, with respect to the "best," ϑ_t, and worst, ϑ_w, solution,

$$\text{relative error} = \frac{\vartheta_i - \vartheta_t}{\vartheta_t - \vartheta_w}. \tag{34}$$

[84] In S2–1, ϑ_t was the average of the obtained U and D_L values of the interpolation method ($\Delta t = 0.001$ and $k = 8$) and the reflection barrier method ($\Delta t = 0.001$ and $k = 1$). This is justified because both methods converged to the same solution. In S2–2 we used the calculated reference RMSE (see the appendix) as the true solution. Figure 12 demonstrates that for each result (apparent average velocity U, apparent longitudinal macrodisperion D_L, RMSE with respect to homogeneous concentration) the improved reflection barrier method represents the method with the highest computational efficiency (the best result for any given CPU time). The higher computational cost of the interpolation method is based on: (1) the expensive bilinear interpolation of $\mathbf{u}$ and θ in each time step for every particle and (2) the calculation of a refined velocity matrix when grid refinement is applied. In scenarios S2–1 and S2–2, the latter step is performed only once as we assumed a steady state velocity field. We stress that the steady state scenario used here is advantageous for the interpolation method. In particular, when dealing with the commonly highly transient flow in soils, in which the velocity field is frequently updated, the calculation of the refined velocity matrix can become a considerable time-consuming factor for the interpolation method. The improved reflection barrier method requires no grid refinement and its computational efficiency is therefore not affected by new velocity fields occurring under transient conditions.

[85] The results of S2–1 and S2–2 (Figures 7 and 9) indicate that a lower parameter variability, and thus a less demanding scenario, reduces the efficiency differences between the reflection barrier and interpolation method. In contrast, a higher variability does not influence the fast convergence of the improved reflection barrier method while the interpolation method has convergence problems even with the finest grid and smallest time step size. Based on these results, we conclude that the reflection barrier method is best suited for hydraulic parameter fields with high contrasts, while it has no disadvantages if the contrasts are lower.

5.3. Practical Application Aspects of the Improved Reflection Barrier Method

[86] The proposed three algorithmic improvements to the reflection barrier method can easily be implemented in a standard RWPT code, as they only need small modifications of the core module responsible for the dispersive displacement of a particle.

[87] The proposed RWPT algorithm is superior to other RWPT algorithms in situations where either the water content or the dispersion tensor are discontinuous. This can be the case when the flow velocity field is obtained from a discretization scheme where the water content is element-wise constant (as, e.g., in cell-centered finite-volume schemes) resulting in abrupt changes of the dispersion tensor (as the pore water velocity is unsteady) and water content at element interfaces. However, even for finite element solutions where the solution is much smoother, discontinuities can occur at material interfaces. Our results showed that the efficiency gain of the reflection barrier method is increasing with the heterogeneity of the system, while the interpolation method has severe problems approaching the true solution.

[88] To obtain convergence with the reflection barrier method, in principle, reflecting barriers have to be applied at all element interfaces with a discontinuity of the dispersion tensor or water content. To reduce the computation time, it might be possible to define a threshold depending on the size of the jump indicating whether or not an

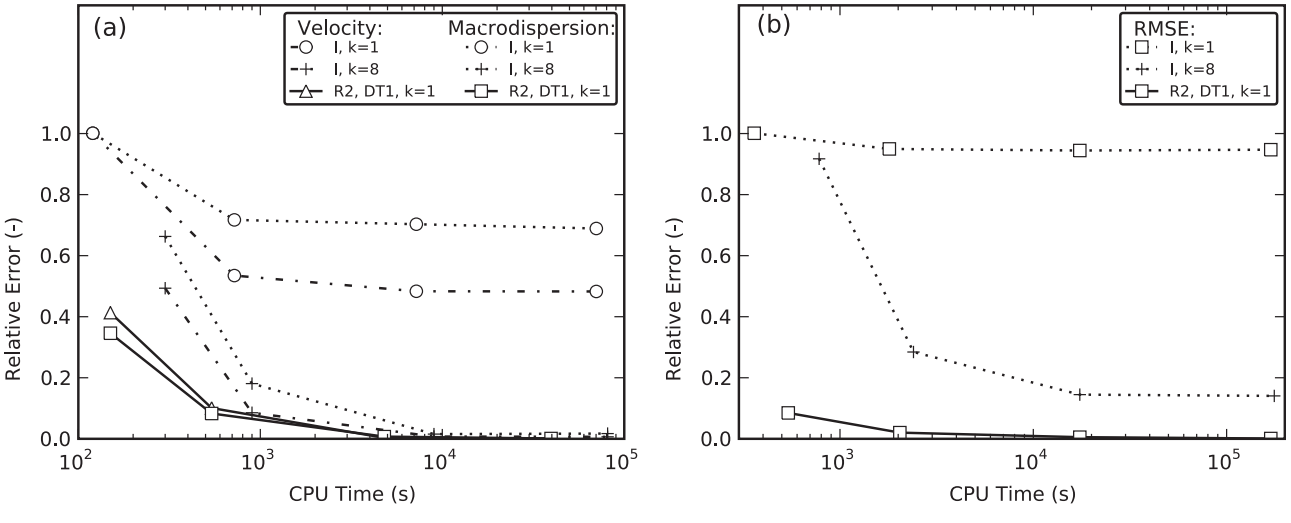

Figure 12. Relative error (equation (34)) as a function of CPU time (s). (a) Scenario S2–1, relative error given for apparent average velocity U and apparent longitudinal macrodispersion D_L. (b) Scenario S2–2, relative error given with respect to best possible RMSE. k: Grid refinement factor, k is the number of subdivisions along each axis of the element of the coarsest grid: R2: one-sided reflection scheme, and I: interpolation method; DT1: transformation of dispersive displacement was applied.

interface should act as a reflection barrier. If a large part of the domain is characterized by negligible jumps between two adjacent elements, this could lead to a marked acceleration of the reflection barrier method. However, the error introduced by the thresholding has to be tested with a convergence analysis for the specific scenario.

6. Conclusions

[89] We presented three improvements to the reflection barrier method used in RWPT algorithms. This method was originally developed to account for discontinuities of the dispersion tensor, but can also be used to account for abrupt changes in the water content and retardation factors as recently proposed by *Lim* [2006].

[90] 1. We showed that a linear time splitting for the dispersive displacement across an element interface with $\Delta t = \Delta t_1 + \Delta t_2$ proposed in the reflection schemes of *Hoteit et al.* [2002] and *Lim* [2006], and applied in subsequent studies [*Salamon et al.*, 2006; *Zhang et al.*, 2009] systematically overestimates the second dispersive displacement. The erroneous linear time splitting caused deviations of numerical results from analytical solutions observed in previous studies [*Salamon et al.*, 2006]. We derived a corrected time splitting with $\sqrt{\Delta t} = \sqrt{\Delta t_1} + \sqrt{\Delta t_2}$.

[91] 2. Our results demonstrate that the two-sided reflection barrier method is only valid for $\Delta t \to 0$ which has been stated differently in previous studies [*Ackerer and Mose*, 2000]. Inaccuracies occur for a discrete time step size. To reduce this error, we derived a one-sided reflection scheme from the two-sided reflection coefficients of *Lim* [2006]. The strength of our new approach is that monotonicity is preserved while the portion of reflected particles is systematically reduced at all element interfaces. Therefore, the error introduced by the reflection barrier method in a discrete time step size Δt is reduced.

[92] 3. In complex multidimensional transport problems with spatially abruptly varying anisotropic dispersion tensors, the reflection barrier method can be improved by a transformation of the dispersive displacement before performing the second dispersive displacement starting from an interface within one time step Δt. We proposed a transformation of the dispersive displacement that is consistent with the definition of the reflection coefficient and assures a proper convergence of the reflection barrier method to the true solution in complex multidimensional transport problems.

[93] The comparison of RWPT simulations in two- and three-dimensional space applying different reflection barrier schemes demonstrated that only the improved reflection barrier method was able to converge to the true solution of the ADE for all scenarios. The improved reflection barrier method also provided more accurate results for a much larger time step size compared to the original reflection barrier schemes. In two- or three-dimensional simulations, where we usually deal with many element interfaces and complex flow and transport problems, significant jumps in the dispersion tensor or water content normally occur only at a small portion of the total number of element interfaces. For these cases, especially the proposed one-sided reflection scheme is very beneficial as it reduces the number of necessary reflections tremendously. We stress that the algorithmic issues and improvements presented here with respect to the reflection barrier method do not apply to the GSDE method.

[94] A comparison with the interpolation method demonstrated that the reflection barrier method in combination with our improvements can provide more efficiently accurate results of the complex three-dimensional transport problems presented in this study. Especially for abrupt changes of the dispersion tensor and unsaturated conditions characterized by highly heterogeneous water contents, the improved reflection barrier method has important advantages since, unlike the interpolation method, it does not require grid refinements to represent discontinuities. In the interpolation method, results improve when refining the grid used for the bilinear interpolation of the variables governing the dispersive displacement. Our results demonstrate that the problems resulting from the application of the reflection barrier method to complex three-dimensional scenarios, which have been reported before [*LaBolle et al.*, 1996; *Salamon et al.*, 2006], can be alleviated effectively using the proper improvements or corrections.

[95] The proposed RWPT algorithm may be very useful in parameter optimization and geostatistical inversion studies for groundwater or vadose zone applications, in which numerous forward model runs need to be performed with acceptable accuracy in short times. We stress that the algorithm combines the good performance of RWPT under advection-dominated transport conditions with an improved treatment of the dispersive transport. Especially for simulations in the vadose zone, where advection- and dispersion-dominated transport conditions alternate, it is important that numerical codes work efficiently under both conditions. However, the new algorithm also enhances the applicability of RWPT to groundwater studies, in which dispersion from or into low velocity zones must be simulated accurately.

Appendix A: Reference RMSE

[96] Let C_i be the concentration in the cell i with the volume ΔV_i and the water content θ_i. If we have $n_{par,tot}$ particles for the entire domain, and if we distribute these particles in the domain in such a way that the concentration C_i in each cell is the same, we have $n_{par,i}$ particles in the cell i:

$$n_{par,i} = n_{par,tot} \frac{\theta_i \Delta V_i}{\sum_i \theta_i \Delta V_i}. \tag{A1}$$

[97] The fraction of particles in the cell i is equal to the probability p_i that a particle is in the cell i,

$$p_i = \frac{n_{par,i}}{n_{par,tot}} = \frac{\theta_i \Delta V_i}{\sum_i \theta_i \Delta V_i} n_{par,tot}^{-1}. \tag{A2}$$

[98] The concentration in the cell i is related to the fraction of particles in the cell i as,

$$C_i = \frac{n_{par,i} M_{par}}{\theta_i \Delta V_i} = \frac{n_{par,tot} M_{par}}{\theta_i \Delta V_i} p_i. \tag{A3}$$

[99] Instead of distributing the $n_{par,tot}$ over the domain so that the concentration is uniform, the particles can also be

distributed according to a random process with a probability p_i that a particle is placed in the cell i. If this random process is repeated for $n_{par,tot}$ particles, the expected value of the fraction of particles in the cell i, f_i, is equal to p_i. The variance of f_i, $\sigma^2_{f,i}$ is

$$\sigma^2_{f,i} = \frac{p_i(1-p_i)}{n_{par,tot}}. \tag{A4}$$

[100] The concentration that is derived from f_i is

$$\hat{C}_i = \frac{n_{par,tot} M_{par}}{\theta_i \Delta V_i} f_i, \tag{A5}$$

where M_{par} is the mass of a single particle. Its expected value is equal to $\hat{C}_i$ and its variance is equal to:

$$\sigma^2_{\hat{C}_i} = \left(\frac{n_{par,tot} M_{par}}{\theta_i \Delta V_i}\right)^2 \frac{p_i(1-p_i)}{n_{par,tot}} = n_{par,tot}\left(\frac{M_{par}}{\theta_i \Delta V_i}\right)^2 p_i(1-p_i). \tag{A6}$$

[101] Using the equation for p_i, this gives:

$$\sigma^2_{\hat{C}_i} = n_{par,tot}\left(\frac{M_{par}}{\theta_i \Delta V_i}\right)^2 \frac{\theta_i \Delta V_i}{\sum_i \theta_i \Delta V_i}\left(1 - \frac{\theta_i \Delta V_i}{\sum_i \theta_i \Delta V_i}\right). \tag{A7}$$

[102] If M_{par} is defined so that the overall average concentration is equal to 1, then M_{par} is equal to:

$$\frac{n_{par,tot} M_{par}}{\sum_i \theta_i \Delta V_i} = 1 \Rightarrow M_{par} = \frac{\sum_i \theta_i \Delta V_i}{n_{par,tot}}. \tag{A8}$$

[103] As a consequence, the expected value of $\hat{C}_i = 1$ and its variance is

$$\sigma^2_{\hat{C}_i} = \frac{1}{n_{par,tot}}\left(\frac{\sum_i \theta_i \Delta V_i}{\theta_i \Delta V_i}\right)^2 \frac{\theta_i \Delta V_i}{\sum_i \theta_i \Delta V_i}\left(1 - \frac{\theta_i \Delta V_i}{\sum_i \theta_i \Delta V_i}\right). \tag{A9}$$

[104] Rewriting this gives:

$$\sigma^2_{\hat{C}_i} = \frac{1}{n_{par,tot}}\left(\frac{\sum_i \theta_i \Delta V_i}{\theta_i \Delta V_i} - 1\right). \tag{A10}$$

[105] The root-mean-square error (RMSE) is the root of the average of the variances in all cells

$$\mathrm{RMSE} = \sqrt{\frac{\sum_i \sigma^2_{\hat{C}_i}}{n_{elements}}}. \tag{A11}$$

[106] **Acknowledgments.** This study was funded by the network EOS (www.netzwerk-eos.dlr.de). We thank Horst Hardelauf who coupled the finite volume flow code to the PARTRACE code and Michael Herbst for the introduction to the PARTRACE code. We thank Colin Kikuchi for his help in improving the English wording.

References

Ackerer, P., and R. Mose (2000), Comment on "Diffusion theory for transport in porous media: Transition-probability densities of diffusion processes corresponding to advection-dispersion equations" by Eric M. LaBolle et al., *Water Resour. Res.*, *36*(3), 819–821, doi:10.1029/1999WR900326.

Ahlstrom, S. W., H. P. Foote, R. C. Arnett, C. R. Cole, and R. J. Serne (1977), Multi-component mass transport model: Theory and numerical implementation., *Rep. BNWL-2127, Battelle Pacific Northwest Lab., Richland, Wash.*

Aris, R. (1956), On the Dispersion of a Solute in a Fluid Flowing through a Tube, *Proc. R. Soc. London*, *235*(1200), 67–77.

Bear, J. (1972), *Dynamics of fluids in porous media*, vol. 17, 764 pp., Elsevier, N. Y.

Bechtold, M., S. Haber-Pohlmeier, J. Vanderborght, A. Pohlmeier, P. A. Ferre, and H. Vereecken (2011), Near-surface solute redistribution during evaporation, *Geophys. Res. Lett.*, *38*, L17404, doi:10.1029/2011GL048147.

Brezzi, F., and M. Fortin (1991), *Mixed and Hybrid Finite Element Methods*, 355 pp., Springer, N. Y.

Coquet, Y., J. Simunek, C. Coutadeur, M. T. van Genuchten, V. Pot, and J. Roger-Estrade (2005), Water and solute transport in a cultivated silt loam soil: 2. Numerical analysis, *Vadose Zone J.*, *4*(3), 587–601, doi:10.2136/vzj2004.0153.

Cordes, C., H. Daniels, and G. Rouvé (1991), A new very efficient algorithm for particle tracking in layered aquifers, in *Computer Methods in Water Resources II, Groundwater Modelling and Pressure Flow*, vol. 1, pp. 41–55, edited by D. B. Sari et al., Springer, Germany.

Delay, F., P. Ackerer, and C. Danquigny (2005), Simulating solute transport in porous or fractured formations using random walk particle tracking: A review, *Vadose Zone J.*, *4*(2), 360–379, doi:10.2136/vzj2004.0125.

Deutsch, C. V., and A. G. Journel (1998), *GSLIB: Geostatistical Software Library and User's Guide*, 2nd ed., 369 pp., Oxford Univ. Press, N. Y.

Fernandez-Garcia, D., T. H. Illangasekare, and H. Rajaram (2005), Differences in the scale-dependence of dispersivity estimated from temporal and spatial moments in chemically and physically heterogeneous porous media, *Adv. Water Resour.*, *28*(7), 745–759, doi:10.1016/j.advwatres.2004.12.011.

Haber-Pohlmeier, S., M. Bechtold, S. Stapf, and A. Pohlmeier (2010), Water flow monitored by tracer transport in natural porous media using magnetic resonance imaging, *Vadose Zone J.*, *9*(4), 835–845, doi:10.2136/vzj2009.0177.

Hoteit, H., R. Mose, A. Younes, F. Lehmann, and P. Ackerer (2002), Three-dimensional modeling of mass transfer in porous media using the mixed hybrid finite elements and the random-walk methods, *Math. Geol.*, *34*(4), 435–456, doi:10.1023/A:1015083111971.

Ippisch, O., H. J. Vogel, and P. Bastian (2006), Validity limits for the van Genuchten-Mualem model and implications for parameter estimation and numerical simulation, *Adv. Water Resour.*, *29*(12), 1780–1789, doi:10.1016/j.advwatres.2005.12.011.

Javaux, M., J. Vanderborght, R. Kasteel, and M. Vanclooster (2006), Three-dimensional modeling of the scale- and flow rate-dependency of dispersion in a heterogeneous unsaturated sandy monolith, *Vadose Zone J.*, *5*(2), 515–528, doi:10.2136/vzj2005.0056.

Kasteel, R., T. Putz, and H. Vereecken (2007), An experimental and numerical study on flow and transport in a field soil using zero-tension lysimeters and suction plates, *Eur. J. Soil Sci.*, *58*(3), 632–645, doi:10.1111/j.1365-2389.2006.00850.x.

Kinzelbach, W., and G. Uffink (1991), The random walk method and extensions in groundwater modelling, in *Transport Processes Porous Med.*, edited by J. Bear and M. Y. Corapcioglu, pp. 761–787, Kluwer, Hingham, Mass.

Kowalsky, M. B., S. Finsterle, and Y. Rubin (2004), Estimating flow parameter distributions using ground-penetrating radar and hydrological measurements during transient flow in the vadose zone, *Adv. Water Resour.*, *27*(6), 583–599, doi:10.1016/j.advwatres.2004.03.003.

LaBolle, E. M., G. E. Fogg, and A. F. B. Tompson (1996), Random-walk simulation of transport in heterogeneous porous media: Local mass-conservation problem and implementation methods, *Water Resour. Res.*, *32*(3), 583–593, doi:10.1029/95WR03528.

LaBolle, E. M., J. Quastel, and G. E. Fogg (1998), Diffusion theory for transport in porous media: Transition-probability densities of diffusion processes corresponding to advection-dispersion equations, *Water Resour. Res.*, *34*(7), 1685–1693, doi:10.1029/98WR00319.

LaBolle, E. M., J. Quastel, G. E. Fogg, and J. Gravner (2000), Diffusion processes in composite porous media and their numerical integration by

random walks: Generalized stochastic differential equations with discontinuous coefficients, *Water Resour. Res.*, *36*(3), 651–662, doi:10.1029/1999WR900224.

Lichtner, P. C., S. Kelkar, and B. Robinson (2002), New form of dispersion tensor for axisymmetric porous media with implementation in particle tracking, *Water Resour. Res.*, *38*(8), 1146, doi:10.1029/2000WR000100.

Lim, D. H. (2006), Numerical study of nuclide migration in a nonuniform horizontal flow field of a high-level radioactive waste repository with multiple canisters, *Nucl. Technol.*, *156*(2), 222–245.

Marle, C., P. Simandou, and C. Gaulier (1967), Etude du déplacement de fluids miscibles en milieu poreux stratifié, *Revue De L Institut Francais Du Petrole Et Annales Des Combustibles Liquides*, *22*(2), 272–294.

Maxwell, R. M., C. Welty, and R. W. Harvey (2007), Revisiting the Cape Cod bacteria injection experiment using a stochastic modeling approach, *Environ. Sci. Technol.*, *41*(15), 5548–5558, doi:10.1021/es062693a.

Maxwell, R. M., A. F. B. Tompson, and S. Kollet (2009), A serendipitous, long-term infiltration experiment: Water and tritium circulation beneath the CAMBRIC trench at the Nevada Test Site, *J. Contam. Hydrol.*, *108*(1–2), 12–28, doi:10.1016/j.jconhyd.2009.05.002.

Miller, E. E., and R. D. Miller (1956), Physical theory for capillary flow phenomena, *J. Appl. Phys.*, *27*(4), 324–332.

Neuendorf, O. (1997), *Numerische 3D-Simulation des Stofftransports in einem heteorgenen Aquifer.*, Res. Center Juelich Publ., Juelich, Germany.

Nowak, W., F. P. J. de Barros, and Y. Rubin (2010), Bayesian geostatistical design: Task-driven optimal site investigation when the geostatistical model is uncertain, *Water Resour. Res.*, *46*(3), W03535, doi:10.1029/2009WR008312.

Park, C. H., C. Beyer, S. Bauer, and O. Kolditz (2008), A study of preferential flow in heterogeneous media using random walk particle tracking, *Geosci. J.*, *12*(3), 285–297, doi:10.1007/s12303-008-0029-2.

Pollock, D. W. (1988), Semianalytical computation of path lines for finite-difference Models, *Ground Water*, *26*(6), 743–750.

Prickett, T. A., T. G. Naymik, and C. G. Longquist (1981), A random walk solute transport model for selected groundwater quality evaluations, *Illinois State Water Surv. Bulletin*, *65*, Champain, IL.

Ramirez, J. M., E. A. Thomann, E. C. Waymire, J. Chastanet, and B. D. Wood (2008), A note on the theoretical foundations of particle tracking methods in heterogeneous porous media, *Water Resour. Res.*, *44*(1), W01501, doi:10.1029/2007WR005914.

Raviart, P. A., and J. M. Thomas (1975), A mixed finite element method for second order elliptic problems, in *Mathematical Aspects of the Finite Element Methods, Lecture Notes in Mathematics 606*, pp. 292–315, Springer, Berlin, Germany.

Rossi, M., O. Ippisch, and H. Flühler (2008), Solute dilution under imbibition and drainage conditions in a heterogeneous structure: Modeling of a sand tank experiment, *Adv. Water Resour.*, *31*(9), 1242–1252, doi:10.1016/j.advwatres.2008.04.003.

Salamon, P., D. Fernandez-Garcia, and J. J. Gomez-Hernandez (2006), A review and numerical assessment of the random walk particle tracking method, *J. Contam. Hydrol.*, *87*(3–4), 277–305, doi:10.1016/j.jconhyd.2006.05.005.

Salamon, P., D. Fernandez-Garcia, and J. J. Gomez-Hernandez (2007), Modeling tracer transport at the MADE site: The importance of heterogeneity, *Water Resour. Res.*, *43*(8), W08404, doi:10.1029/2006WR005522.

Samouelian, A., H. J. Vogel, and O. Ippisch (2007), Upscaling hydraulic conductivity based on the topology of the sub-scale structure, *Adv. Water Resour.*, *30*(5), 1179–1189, doi:10.1016/j.advwatres.2006.10.011.

Schafer-Perini, A. L., and J. L. Wilson (1991), Efficient and accurate front tracking for 2-dimensional groundwater-flow models, *Water Resour. Res.*, *27*(7), 1471–1485, doi:10.1029/91WR00720.

Seeboonruang, U., and T. R. Ginn (2006), Upscaling heterogeneity in aquifer reactivity via exposure-time concept: Forward model, *J. Contam. Hydrol.*, *84*(3–4), 127–154, doi:10.1016/j.jconhyd.2005.12.011.

Semra, K., P. Ackerer, and R. Mose (1993), Three dimensional Groundwater Quality Modeling in Heterogeneous Media, in *Water Pollution II: Modelling, Measuring and Prediction*, edited by L. C. Wrobel and C. A. Brebbia, pp. 3–11, Southampton, U. K.

Tompson, A. F. B., and L. W. Gelhar (1990), Numerical-simulation of solute transport in 3-dimensional, randomly heterogeneous porous-media, *Water Resour. Res.*, *26*(10), 2541–2562, doi:10.1029/WR026i010p02541.

Uffink, G. J. M. (1985), A random-walk method for the simulation of macrodispersion in a stratified aquifer, *IAHS symposia, IUGG 18th general assembly*, *65*, 26–34.

Weissmann, G. S., Y. Zhang, E. M. LaBolle, and G. E. Fogg (2002), Dispersion of groundwater age in an alluvial aquifer system, *Water Resour. Res.*, *38*(10), 1198, doi:10.1029/2001WR000907.

Zhang, Y., E. M. LaBolle, and K. Pohlmann (2009), Monte Carlo simulation of super diffusion and subdiffusion in macroscopically heterogeneous media, *Water Resour. Res.*, *45*, W10417, doi:10.1029/2008WR007448.

M. Bechtold, J. Vanderborght, and H. Vereecken, Agrosphere (IBG-3), Institute of Bio- and Geosciences, Forschungszentrum Jülich GmbH, Leo Brandt Straße, 52425 Jülich, Germany. (michel.bechtold@vti.bund.de)

O. Ippisch, Interdisciplinary Center of Scientific Computing, University of Heidelberg, Im Neuenheimer Feld 368, 69120 Heidelberg, Germany.